Butyrate Ameliorates Graves' Orbitopathy Through Regulating Orbital Fibroblast Phenotypes and Gut Microbiota

Pingbo Ouyang,[1] Jia Qi,[2] Boding Tong,[1] Yunping Li,[1] Jiamin Cao,[3] Lujue Wang,[1] Tongxin Niu,[1] and Xin Qi[1]

[1]Department of Ophthalmology, The Second Xiangya Hospital, Central South University, Changsha, Hunan, China
[2]Department of Anesthesiology, The Second Xiangya Hospital, Central South University, Changsha, Hunan, China
[3]Department of Ophthalmology, The Third Xiangya Hospital, Central South University, Changsha, Hunan, China

Correspondence: Xin Qi, Department of Ophthalmology, the Second Xiangya Hospital, Central South University, Changsha, Hunan 410011, China; qixin78@csu.edu.cn.

PO and JQ contributed equally to this work.

Received: August 7, 2024
Accepted: February 4, 2025
Published: March 4, 2025

Citation: Ouyang P, Qi J, Tong B, et al. Butyrate ameliorates graves' orbitopathy through regulating orbital fibroblast phenotypes and gut microbiota. *Invest Ophthalmol Vis Sci.* 2025;66(3):5. https://doi.org/10.1167/iovs.66.3.5

Purpose. Graves' orbitopathy (GO), the common extrathyroidal complication of Graves' disease (GD), is characterized by orbital fibroblast stimulation, adipogenesis, and hyaluronan production. Recently, gut microbiota and its metabolites have garnered attention for their possible involvement in GO.

Methods. This study utilized an animal model of GO and examined the effects of butyrate treatment on orbital fibroblast cells and gut microbiota. Ex vivo experiments were performed using orbital fibroblasts derived from healthy patients' and patients' with GO orbital tissue to evaluate vitality, activation, and adipogenesis in response to butyrate treatment. Gut microbiota diversity was also analyzed in butyrate-treated and untreated GO mice.

Results. In human orbital fibroblasts, butyrate treatment dramatically decreased the vitality of GO-derived fibroblasts without harming normal fibroblasts. Butyrate prevented activation and fibrotic processes induced by transforming growth factor beta 1 (TGF-β1) in GO and normal fibroblasts. Additionally, butyrate reduced lipid droplet formation and downregulated lipogenic markers in GO and normal orbital fibroblasts, inhibiting adipogenesis. In the GO mouse model, butyrate therapy improved orbital histological abnormalities and normalized serum thyroid hormone and antibody levels. The intestinal microbiome of butyrate-treated GO mice also changed significantly, with a reduction in certain bacteria (Bifidobacterium, GCA-900066575, and Parabacteroides) and an increase in others (Bacteroides and Rikenellaceae_RC9).

Conclusions. Butyrate ameliorates several of the symptoms of GO, lowering GO orbital fibroblast viability, adipogenesis, and TGF-β1-induced fibrosis without damaging normal fibroblasts. Butyrate normalizes thyroid function in a GO mouse model, improves histopathological alterations, and transforms gut microbiota populations, proving its potential in treating GO through the gut-thyroid axis.

Keywords: graves' orbitopathy (GO), orbital fibroblast, butyrate, adipogenesis, gut microbiota

Graves' orbitopathy (GO), also referred to as Graves' ophthalmopathy, represents the most prevalent extrathyroidal complication of Graves' disease (GD).[1–4] Characterized by enhanced adipogenesis in orbital fibroblasts and hyaluronan synthesis, GO predominantly manifests through extensive orbital tissue remodeling, evidenced by adipose tissue enlargement and tissue edema.[5–7] This remodeling further leads to clinical symptoms such as eye redness, swelling, diplopia, proptosis, and blurred vision.[8–10] Given the significant morbidity and economic burden associated with GO, comprehensive management strategies focusing on early detection and targeted intervention are essential to mitigate its impact on patient health and healthcare systems.

Traditionally, genetic background, in conjunction with environmental factors including stress, smoking, and pregnancy, along with bacterial infections and immune responses to food and other antigens, collectively contribute to an increased predisposition to GD and GO.[11–14] Recently, considering that GO is an autoimmune disorder,[15,16] the underlying effect of gut microbiota on the occurrence of GO has emerged as a significant area of research since the interdependent interaction between gut microbiota and host immunity has been reported.[17] The gut, as a key regulator of microbiological, physiological, and physical homeostasis, enables the host to withstand various infections and environmental stressors.[18] The gastrointestinal tract has the highest concentration of resident immune cells because it has the

largest surface area between the external environment and the internal tissue and is exposed to a variety of infectious and non-infectious stressors. A complex network of innate and adaptive components, the mucosal immune system responds well to many environmental stressors.[19] Symbiotic microbiota exerts a crucial effect on shaping and modulating these immune responses, training, and fine-tuning the immune system's functionality.[20,21] Regarding GD/GO, an association between the intestinal microbiota and autoimmune thyroid has been reported in GO mouse models.[22,23] A change in beta diversity of bacterial communities in thyroid-stimulating hormone receptor (TSHR)-immunized group in comparison with the control group was observed, as well as a positive relationship between *Firmicutes* and orbital adipogenesis.[22,24] Alterations in the intestinal microbiota, however, have a significant impact on measurable GD endocrine and immunological factors, whereas the effect on GO cellular alterations is more subtle.[25] Therefore, the effect of gut microbiota on GO pathogenesis requires further investigation.

The microbiota and its metabolites have been previously reported to impact the functions of the gut barrier, releasing the metabolites and other factors into the systemic circulation.[26,27] Specifically, butyrate exerts a significant effect on regulating intestinal homeostasis, particularly in the context of thyroid disorders; butyrate-producing microbiotas were found to be reduced in patients with GD and hypothyroidism in comparison with the control group.[28] In addition, the focus on butyrate arises from its production by *Faecalibacterium prausnitzii*, a species uniquely identified with the genus *Faecalibacterium*, which exerts a pivotal effect on maintaining intestinal immune homeostasis. *Faecalibacterium prausnitzii* is known to suppress the nuclear factor kappa-B and T helper cell 17/interleukin-17 pathways.[29–31] In our previous study, the abundance of *Faecalibacterium prausnitzii* in the gut has also been proven to be different among healthy people and patients with different degrees of GO severity.[32] Butyrate, as produced by this bacterium, helps regulate oxidative stress, reduces peroxidase and cyclooxygenase activities, and inhibits the expression of inflammatory cytokines, effectively alleviating inflammatory responses along the lining of the gut.[33] More importantly, regarding the activation of fibroblasts, sodium butyrate has been reported to improve skin or pulmonary fibrogenesis and the imbalance of bacteria in the intestines within bleomycin-induced murine models.[34] Butyrate also regulates macrophage M1/M2 polarization and promotes mitochondrial function recovery to improve cardiac fibrosis.[35] Regarding adipogenesis, sodium butyrate supplements could inhibit liver steatosis and lipogenesis in high-fat diet-treated mice.[36] Therefore, the reduced levels of butyrate might be key to critical physiological processes in the pathogenesis of GO, warranting a deeper exploration of butyrate's role in this context.

In this study, primary orbital fibroblasts were extracted from orbital tissue samples of patients with GO and healthy controls, and the specific effects of butyrate upon the viability, proliferation, fibrogenesis, and lipogenesis of different fibroblasts were investigated. A GO model was established in mice and the in vivo effects of butyrate on GO mice were investigated. Last, the effects of butyrate on the gut microbiota of the model mice were investigated. Collectively, the aim of this study is to elucidate the comprehensive effect of butyrate on modulating GO pathophysiology, from cellular mechanisms in fibroblasts to systemic effects in animal models, and its potential influence on gut microbiota composition, thereby contributing to an improved comprehension of the gut-thyroid axis in GO.

Materials and Methods

Clinical Sample Collection

Healthy control upper eyelid's orbital connective tissues were obtained from healthy volunteers ($n = 5$, female/male = 3/2, 45.8 ± 8.76 years) with no inflammatory and thyroid conditions and undergoing blepharoplasty. GO upper eyelids orbital tissue specimens were obtained from patients with GO ($n = 5$, inactive disease stage, female/male = 2/3, 44.2 ± 8.44 years) during orbital decompression surgery. All the participants have provided written informed consent in compliance with the principles of the Declaration of Helsinki. This study was conducted under the approval of the ethics committee from the Second Xiangya Hospital.

Primary Orbital Fibroblast Isolation, Identification, and Treatment

The primary cultures of orbital fibroblasts were isolated from orbital tissues as previously described.[37] Briefly, both GO and healthy orbital tissue samples were obtained as above mentioned. The tissues were placed in culture dishes, and covered with complete medium (Dulbecco's Modified Eagle's Medium [DMEM] plus 10% fetal bovine serum [FBS] and 1% penicillin-streptomycin solution [Gibco, USA]). The explanted tissue samples were then incubated in cell culture incubator at 37°C in 5% CO_2. The fibroblasts that grew out of the explants formed monolayers. The resulting fibroblast monolayers were passaged serially by gentle treatment using trypsin/ ethylenediaminetetraacetic acid (EDTA; Gibco, Paisley, UK), and cultivated within DMEM (Gibco) containing 10% FBS and antibiotics (penicillin and streptomycin; BioWhittaker, Verviers, Belgium).[38] The orbital fibroblasts between the second and sixth passages were utilized for the experiments.

Regarding orbital fibroblast identification, immunofluorescence staining was carried out as per the methods described before[39] with antibodies against vimentin, desmin, S100B, and Keratin 17 as the primary antibodies (dilution 1:100), fluorescein isothiocyanate-conjugated secondary antibody (dilution 1:200). The antibodies' information is listed in Supplementary Table S1. The orbital fibroblast exhibited vimentin-positive, desmin, S100B, and Keratin 17 negative.

For orbital fibroblast activation, the GO orbital fibroblasts were stimulated with transforming growth factor beta 1 (TGF-β1; 10 ng/mL, Sangon, Shanghai) for 24 hours. For adipogenic differentiation of orbital fibroblasts, the GO orbital fibroblasts were cultured with a commercial adipogenic differentiation medium (SALIAI, Guangzhou, China) for 10 days for Oil red staining or for 4 days for mRNA and protein expression analysis, the medium was replaced every 3 days. For determination of the function of butyrate in fibroblast activation, orbital fibroblasts were treated with 50 µM butyrate for 24 hours. For determination of butyrate in adipogenic differentiation, orbital fibroblasts were treated with 10 µM butyrate and underwent adipogenic differentiation simultaneously for 10 days or 4 days.

Investigative Ophthalmology & Visual Science

Cell Counting Kit-8 Assay

Two types of orbital fibroblasts were treated with 0, 0.5, 1, 5, 10, 25, 50, and 100 µM butyrate for 24, 48, or 72 hours and a Cell Counting Kit 8 (CCK-8) assay kit (Beyotime) was applied to examine cell viability. At the indicated culture time point, CCK-8 solution at a dilution of 1/10 was supplemented into the medium, followed by 4 hours of incubation. Subsequently, the OD value of each well was detected at 450 nm using a multi-function microplate reader (Bio-Rad, USA).

EdU Assay

DNA synthesis was examined using an incorporation assay, utilizing the Cell Light EdU DNA Imaging Kit (RiboBio Co., Guangzhou, China). The cells were first planted onto 24-well plates and then treated with butyrate (50 µM for 24 hours) and/or TGF-β1 (10 ng/mL, for 24 hours), followed by 2-h exposure to EdU. Subsequently, 4% paraformaldehyde was used to fix cells and 0.5% Triton X-100 was used to permeabilize the cells. Finally, the cells were incubated with reaction solution for 30 minutes in the dark followed by 4′,6-diamidino-2-phenylindole (DAPI) staining for 5 minutes in the dark. A fluorescent microscope was applied to capture fluorescent images. The EdU-positive cells (red fluorescence) were counted by Image J software (NIH, BD, USA). This procedure was independently replicated three times for consistency.

Scratch Wound Healing Assay

Orbital fibroblasts were planted onto 6-well plates at a density of 1×10^5 cells/well. Upon reaching confluence, a sterile 200 µL disposable micropipette tip was utilized to create a straight-line scratch. After two washings in PBS, cellular debris was eliminated, and cultures were subjected to butyrate (50 µM for 24 hours) and/or TGF-β1 (10 ng/mL, for 24 hours) incubation. An inverted phase-contrast microscope was used to photograph the defined microscopic scratch wound areas at the designated time points. The migration distance rate was measured by Image J software.[40]

Immunoblotting

All primary antibodies used are listed in Supplementary Table S1. Cell lysates and tissue homogenates were separated on 10% SDS-PAGE before being transferred onto nitrocellulose membranes, as previously described.[41] Membranes were blocked for 12 hours in 5% skimmed milk tris-buffered saline (TBS) buffer, followed by an overnight incubation at 4°C with primary antibodies against vimentin, fibronectin, collagen I, collagen III, α-SMA, c/EBPα, c/EBPβ, PPARγ, perilipin-1, FABP4, leptin, or adiponectin. Antibodies against GAPDH or β-actin were set as the endogenous control. Membranes were washed, followed by a 1 hour incubation at room temperature (RT) with horseradish peroxidase-labeled secondary antibody (1:5000). The chemiluminescence reagents (Pierce ECL Western Blotting Substrate; Invitrogen, Carlsbad, CA, USA) were used to detect protein bands, and densitometric analysis with Image J software was carried out to quantify the protein bands.

Quantitative RT-PCR

TRIzol reagent (Invitrogen) was used as per the protocol to extract total RNA. The SYBR green PCR Master Mix (Qiagen, Germany) was applied as per the instructions to detect RNA expression levels, with GAPDH utilized as an endogenous control. The $2^{-\Delta\Delta Ct}$ values indicated the relative fold changes. The primer sequence is listed in Supplementary Table S2.

Collagen I Content Determination

After being treated with butyrate (50 µM for 24 hours) and/or TGF-β1 (10 ng/mL, for 24 hours), the cell culture supernatant was collected for collagen I level measurement by ELISA kit (CSB-E08082h) following the instructions of the manufacturer. Finally, after adding the stop solution, the OD value at 450 nm was recorded and the concentration was calculated according to the standard curve.

Oil-Red O Staining

Regarding Oil-Red O staining for orbital fibroblasts, the cells were planted onto 6-well plates (2×10^6 cells/well) and treated with 10 µM butyrate in adipogenic differentiation medium for 10 days. Prior to staining, the cells were subjected to 2 washings in 1 × PBS, 10-minute fixation in 3.7% formaldehyde, and then 3 washings in cold water. After a 30-minute staining at 25°C with a solution of Oil Red O (6:4, 0.6% Oil Red O dye in isopropanol: water), the cells were rinsed thrice in water. The bright-field microscopy was used to visualize staining.

GO Model in Mice

Six to 8 week-old specific pathogen-free (SPF) female BALB/c mice were obtained from Hunan SLAC Laboratory Animal Co. Ltd. and utilized in the present study, reflecting the greater female prevalence of GO, with prior research indicating a more stable GO model within female BALB/c mice.[42,43] The handling of all mice complied with the Guide for the Care and Use of Laboratory Animals, and the procedures were approved by the Ethics Committee of the Second Xiangya Hospital. The mice were allocated into three groups: normal (n = 6), GO (n = 6), and GO + Butyrate (100 mM; Sigma-Aldrich, St. Louis, MO, USA; $n = 6$). Mice in the GO + Butyrate group were given a final concentration of 100 mM Butyrate[44] in their daily drinking water. Concurrently with Butyrate administration, GO was induced using adenovirus expressing the TSHR A subunit as previously described.[23] Briefly, in the GO and GO + butyrate groups, the mice were intramuscularly injected with TSHR-adenovirus (Oribio, Changsha, China) at 0, 3, 6, 9, and 12 weeks. In the GO + butyrate groups, their daily drinking water contained a final concentration of 100 mM butyrate[44] from 0 week to the end of the experiments. Mice in the control group were injected with the same dosage empty-loaded adenovirus (Ori-bio). The control and GO groups reviewed daily pure drinking water. Mice were kept under conventional breeding environment in a 12 hour/12 hour cycle of light and dark. Free access to food and water was given. At the 15 weeks, the mice fecal samples were collected in a clean container and then frozen and stored at –80 °C for 16s rDNA sequencing. After mice were sacrificed under anesthesia, the serum was collected for ELISA and the complete orbital tissues and

thyroid tissues were harvested for histopathological examination and protein expression examination.

Magnetic Resonance Imaging Scanning

On the sampling day, 7.0T magnetic resonance imaging (MRI) scanning was performed to examine the orbits and extraocular muscles (the eyes and the frontal area of the brain) of the mice. The mice were anesthetized before setting all parameters.[45]

Histopathological Examination

The histological examination was conducted as per standard protocols.[46,47] In short, completely dissected orbital tissues and thyroid gland tissues were fixed in 10% buffered formalin and paraffin-embedded, tissue sections from orbital slices were subjected to hematoxylin and eosin (H&E) and Masson staining. An Olympus microscope was used to capture section images. The relative collagen area of each orbit was calculated by digitized image analysis with the optic nerve (ON) as an anatomic landmark. The cross-sectional area of the orbital fat and collagen was normalized to the ON area of each mouse. The thyroid gland tissue slices were subjected to H&E staining to observe the pathological changes.

Immunohistochemical Staining

The immunohistochemical (IHC) staining was performed to evaluate α-SMA and FABP4 levels in mice orbital tissues. Paraffin-embedded orbital tissue sections were deparaffinized in xylene, rehydrated through a graded ethanol series, and subjected to antigen retrieval by boiling in citrate buffer (pH 6.0) for 15 minutes. Endogenous peroxidase activity was blocked using 3% hydrogen peroxide for 10 minutes at RT. The sections were then incubated with a blocking solution (5% bovine serum albumin) for 30 minutes. Primary antibodies against α-SMA (dilution 1:15000) and FABP4 (dilution 1:2000) were diluted according to the manufacturer's instructions and applied to the sections overnight at 4°C. Following primary antibody incubation, the sections were washed with phosphate-buffered saline (PBS) and incubated with IHC Prep & Detect Kit (PK10019; Proteintech). The signal was visualized using a diaminobenzidine (DAB) substrate, and the sections were counterstained with hematoxylin. Images were captured using a light microscope, and the staining intensity and area were quantified using Image J software.

Serum Levels of Thyroid Function Markers

Serum levels of Thyroxine (T4), TSAb, thyroid-stimulating hormone (TSH), TSH-stimulation blocking antibody (TSBAb), triiodothyronine (T3), and free T4 (FT4) in mice from different groups were determined using corresponding enzyme-linked immunosorbent assay (ELISA) kits listed in Supplementary Table S1 following the manufacturers' instructions.

The 16S rDNA Sequencing for Microbial Community Diversity Analysis

The QIAamp Fast DNA Stool Mini Kit (Qiagen, Germany) was used as per the procedure of the manufacturer to extract DNA from fecal specimens. The universal primers 338F (ACTCCTACGGGAGGCAGCA) and 806R (GGACTACHVGGGTWTCTAAT) were designed from the conserved nucleotide sequences upon the bacterial 16S rRNA gene V3-V4 fragment. Next, the V3-V4 fragment sequence was amplified with polymerase chain reaction (PCR) and sequenced upon the Illumina NovaSeq system (Illumina, San Diego, CA, USA), as previously described.[48] The QIIME software (version 1.9) was applied to pre-process and analyze the raw data. UCHIME was utilized to filter out low-quality reads. Clean-tags were obtained after removing the barcode sequence and primer sequence at both ends of the tags and the chimera. The overlapping PE clean-tags were merged into one sequence. Next, the QIIME software was applied to group sequence reads into operational taxonomic units (OTUs) at the 97% similarity level. The abundances of all OTUs within all samples were analyzed, preliminarily reflecting the species richness in the sample.

Alpha and Beta Diversity Indexes

Alpha diversity refers to the richness, diversity, and evenness of species within a community. Sob, Chao, abundance-based coverage estimator (ACE), Shannon, Simpson, and goods-coverage indexes were used in this study. Beta diversity refers to the heterogeneity in species composition across communities, which can be defined as the extent of species replacement along environmental gradients. The principal coordinate analysis (PCA) and nonmetric multidimensional scaling (NMDS) are usually used to assess Beta diversity. R language and QIIME software were applied to perform these analyses.

Microbiota Function Prediction Analysis

PICRUSt 2.0 function prediction analysis was carried out on the biom file obtained by QIIME software. The function of gut microbiota was predicted in combination with the Kyoto Encyclopedia of Genes and Genomes (KEGG) database.[49]

Statistical Analysis

SPSS version 17.0 statistical software was applied to process experimental data. All data were analyzed in triplicate from at least three independent experiments, and the results were summarized in terms of the average (mean $\pm$ SD). Comparisons among the groups were assessed using a Student's *t*-test. Comparisons among groups were assessed using Kruskal-Wallis or 1-way analysis of variance (ANOVA) followed by Tukey's post hoc test. A P value greater than 0.05 means that no effect was observed.

Results

Effects of Butyrate on Human-Derived Orbital Fibroblast Cell Viability

For orbital fibroblast isolation, orbital tissues were collected from healthy donors and patients with GO and verified for histopathological alterations using H&E and Masson staining. Supplementary Figure S1A shows that in GO orbital tissues, more collagen deposits between orbital fat, and larger adipocyte size were observed. Then, the orbital fibroblasts were isolated from the healthy donors' or the patients' with GO orbital tissues and identified using immunofluo-

Investigative Ophthalmology & Visual Science

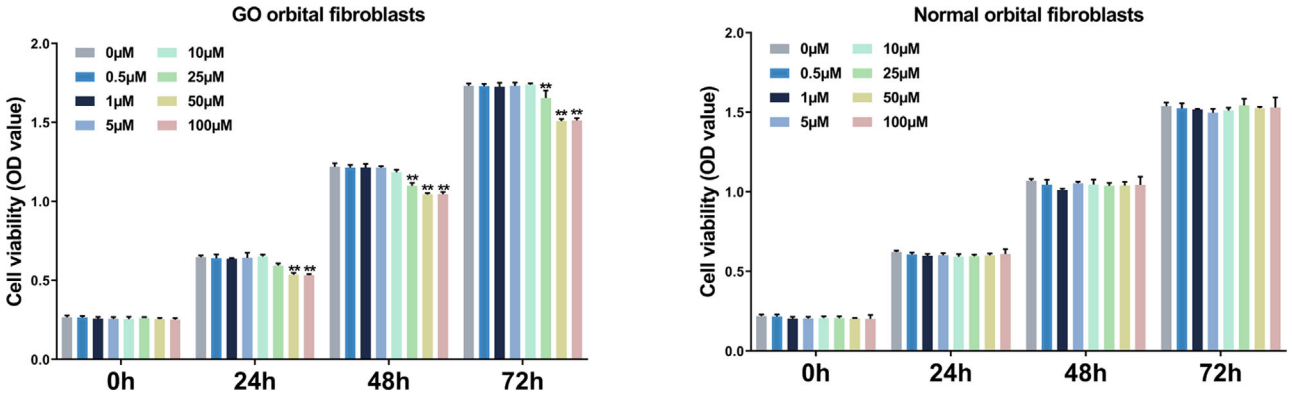

Figure 1. Effects of butyrate on orbital fibroblast cell viability. Orbital fibroblasts isolated from healthy donors' or patients with Graves' orbitopathy (GO) orbital tissues were treated with 0, 0.5, 1, 5, 10, 25, 50, and 100 μM butyrate for 24, 48, or 72 hours and examined for cell viability using a Cell Counting Kit-8 (CCK-8) assay kit ($n = 3$, $^{**}P < 0.01$).

rescence (IF) staining detecting vimentin, desmin, S100B, and keratin 17; Supplementary Figure S1B shows that orbital fibroblasts were vimentin-positive, desmin-negative, S100B-negative, and keratin 17-negative.

Next, isolated orbital fibroblasts were treated with 0, 0.5, 1, 5, 10, 25, 50, and 100 μM butyrate for 24, 48, or 72 hours, and examined for the cytotoxicity of butyrate on healthy and GO orbital fibroblasts. Figure 1 shows that all concentrations of butyrate caused no changes in healthy orbital fibroblast cell viability; 50 and 100 μM butyrate significantly inhibited GO orbital fibroblast cell viability starting from 24 hours and longer treatment, and 25 μM butyrate significantly inhibited GO orbital fibroblast cell viability starting from 48 hours and longer treatment. Then, 50 μM butyrate treatment for 24 hours was applied. The application was used in determining the function of butyrate in orbital fibroblast activation.

Effects of Butyrate Upon the Activation of Human-Derived Orbital Fibroblasts

The specific effects of butyrate upon the activation of human-derived GO orbital fibroblasts were then explored. As for the activation of fibroblasts, GO orbital fibroblasts were exposed to a standard culture medium or induction culture medium containing TGF-β1 (10 ng/mL for 24 hours). Figures 2A to 2D shows that in standard culture medium, butyrate significantly suppressed GO orbital fibroblast proliferation and migration; TGF-β1 stimulation significantly facilitated GO orbital fibroblast proliferation and migration, which was partially suppressed by butyrate treatment. Regarding fibroblast activation markers, butyrate decreased vimentin, fibronectin, collagen I, collagen III, and α-SMA mRNA, and protein expression in GO orbital fibroblast; TGF-β1 stimulation significantly elevated mRNA and protein expression of these markers, which were partially decreased by butyrate treatment (Figs. 2E, 2F). In addition, the concentration of collagen I in the culture medium was decreased by butyrate but increased by TGF-β1 stimulation; the elevation of collagen I concentration by TGF-β1 stimulation was partially abolished by butyrate compared with the single TGF-β1 stimulation group (Fig. 2G). Therefore, butyrate inhibits TGF-β1-induced activation of GO orbital fibroblasts and fibrotic processes.

The impact of butyrate on human-derived normal orbital fibroblast activation was evaluated by treating these cells with TGF-β1 (10 ng/mL for 24 hours) in the presence or absence of butyrate (50 μM). The proliferation of normal orbital fibroblasts was significantly increased following TGF-β1 stimulation, as indicated by the elevated percentage of EdU-positive cells, whereas butyrate treatment effectively reduced this proliferation to levels comparable to unstimulated cells (Figs. 3A, 3B). Similarly, TGF-β1 stimulation enhanced the migratory capacity of normal orbital fibroblasts, as observed in the scratch wound healing assays, whereas butyrate supplementation significantly suppressed this migration (Figs. 3C, 3D). In terms of fibroblast activation markers, TGF-β1 significantly upregulated the protein levels and mRNA expression of vimentin, fibronectin, collagen I, collagen III, and α-SMA (Figs. 3E, 3F). Additionally, collagen I concentration in the culture medium was markedly elevated in response to TGF-β1 stimulation (Fig. 3G). Butyrate treatment reduced the TGF-β1-induced expression of these activation markers and decreased collagen I concentration, indicating that butyrate inhibits fibroblast activation in healthy orbital fibroblasts. Importantly, butyrate treatment alone caused no significant alterations in healthy orbital fibroblast proliferation, migration, and fibrotic marker levels, suggesting that butyrate alone has no cytotoxicity to healthy orbital fibroblasts.

Effects of Butyrate on the Adipogenesis of Human-Derived Orbital Fibroblasts

Considering that GO is characterized by enhanced adipogenesis in orbital fibroblasts and hyaluronan synthesis,[5–7] the effects of butyrate upon the adipogenesis of human-derived orbital fibroblasts were also explored. GO orbital fibroblasts were cultivated in standard or adipogenesis-inducing culture medium, with or without butyrate (10 μM), and examined for cell phenotypes and markers at specific time points. Compared with the non-treatment group, the lipid droplet formation was significantly induced by adipogenesis-inducing culture medium and partially suppressed by butyrate treatment (Fig. 4A). The c/EBPα, c/EBPβ, PPARγ, perilipin-1, FABP4, leptin, and adiponectin mRNA and protein expression were significantly decreased by butyrate but increased by adipogenesis-inducing culture

Investigative Ophthalmology & Visual Science

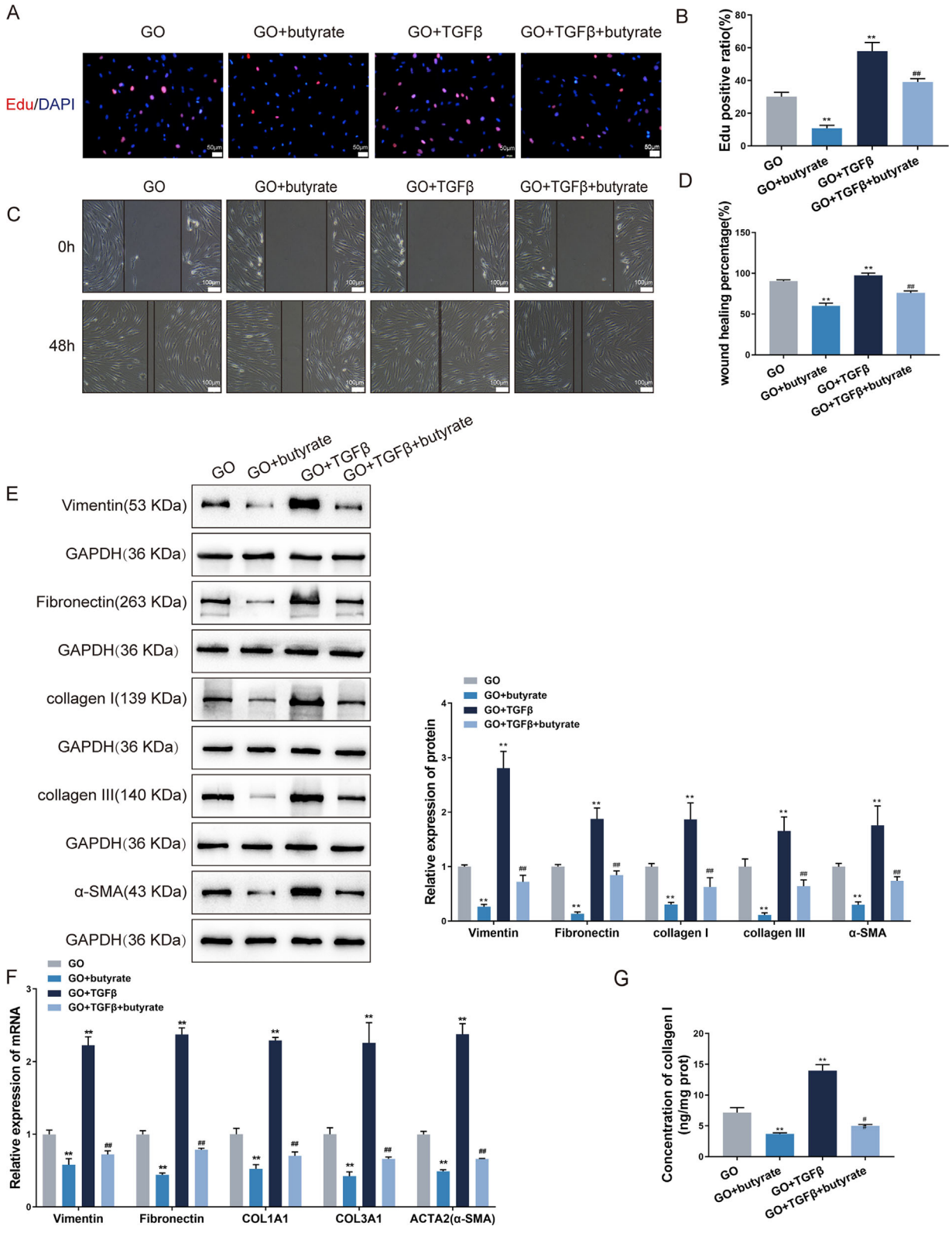

Figure 2. Effects of butyrate on GO orbital fibroblast activation. GO orbital fibroblasts were treated with butyrate (50 μM for 24 hours) and/or TGF-β1 (10 ng/mL, for 24 hours) and examined for cell proliferation using EdU assay (**A, B**); cell migration using scratch wound healing assay (**C, D**); the protein levels of vimentin, fibronectin, collagen I, collagen III, and α-SMA using immunoblotting (**E**); the mRNA expression of vimentin, fibronectin, collagen I, collagen III, and α-SMA using qRT-PCR (**F**); the concentration of collagen I using collagen I kit (**G**) ($n = 3$, $^{**}P < 0.01$ vs. the GO group; $^{\#\#}P < 0.01$ vs. the GO + TGFβ1 group).

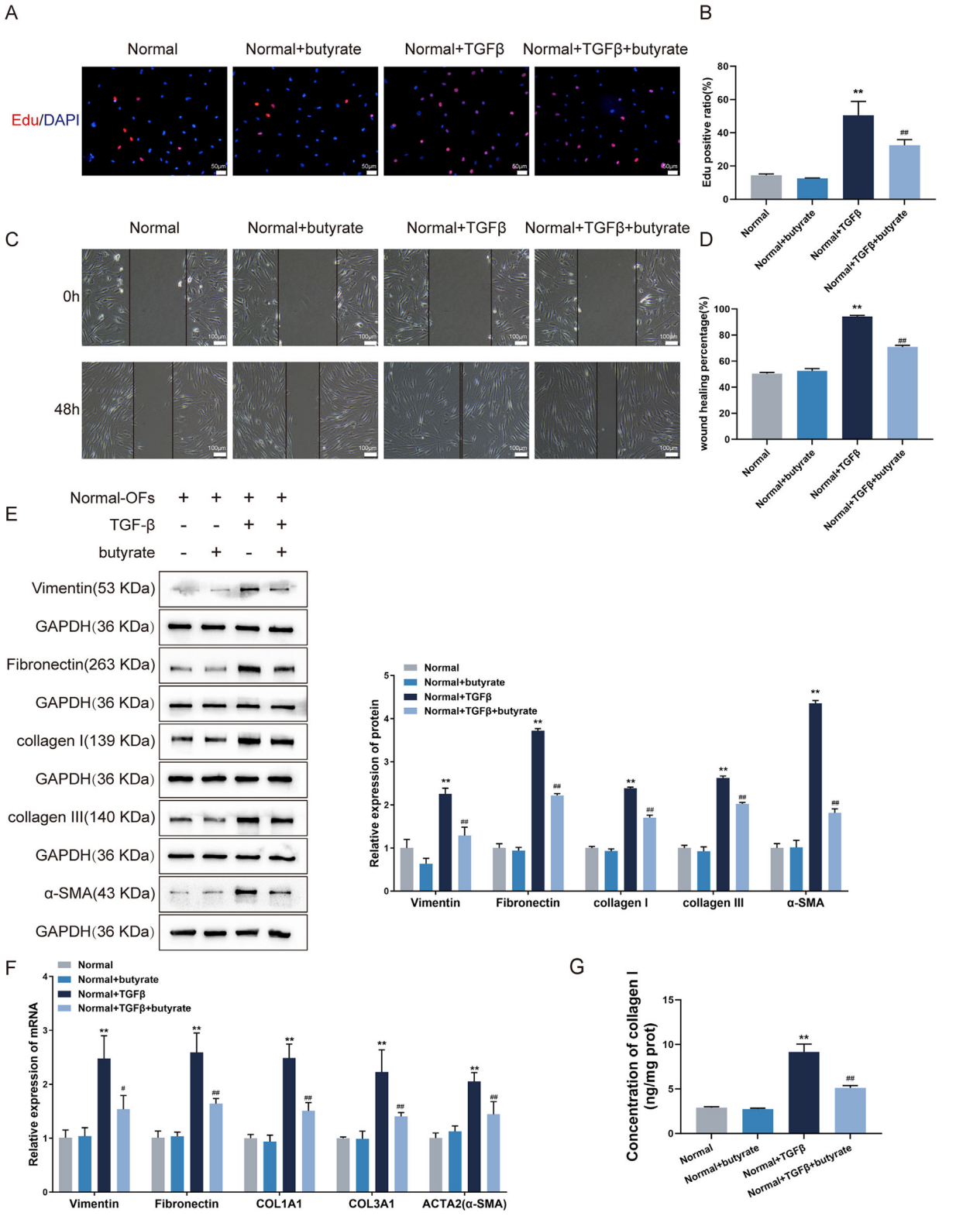

Figure 3. Effects of butyrate on normal orbital fibroblast activation. Normal orbital fibroblasts were treated with butyrate (50 μM for 24 hours) and/or TGF-β1 (10 ng/mL, for 24 hours) and examined for cell proliferation using the EdU assay (**A, B**); cell migration using the scratch wound healing assay (**C, D**); the protein levels of vimentin, fibronectin, collagen I, collagen III, and α-SMA using immunoblotting (**E**); the mRNA expression of vimentin, fibronectin, collagen I, collagen III, and α-SMA using qRT-PCR (**F**); the concentration of collagen I using a collagen I ELISA kit (**G**) ($n = 3$, $^{**}P < 0.01$ vs. the healthy group; $^{\#\#}P < 0.01$ vs. the healthy + TGF-β1 group).

Investigative Ophthalmology & Visual Science

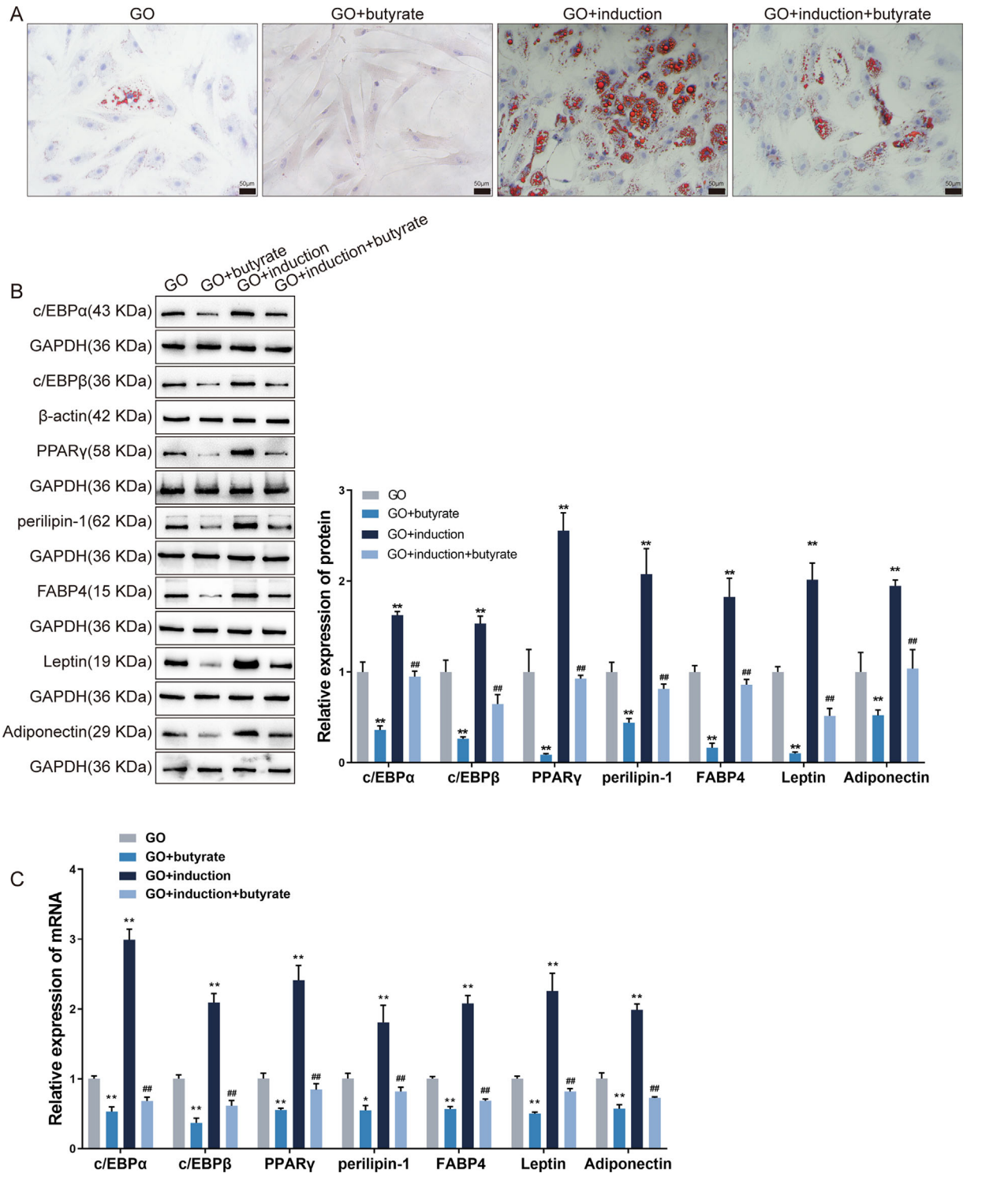

Figure 4. Effects of butyrate on GO orbital fibroblast adipogenesis. GO orbital fibroblasts were cultivated in standard or adipogenesis-inducing culture medium, with or without butyrate (10 µM), and examined for lipid droplet formation using Oil-Red O staining (induction for 10 days) (**A**); the protein levels of c/EBPα, c/EBPβ, PPARγ, perilipin-1, FABP4, leptin, and adiponectin using immunoblotting (**B**); the mRNA expression levels of c/EBPα, c/EBPβ, PPARγ, perilipin-1, FABP4, leptin, and adiponectin using qRT-PCR (**C**) (induction for 4 days, $n = 3$, $^{**}P < 0.01$ vs. the GO group; $^{\#\#}P < 0.01$ vs. the GO + induction group).

Investigative Ophthalmology & Visual Science

medium; the promotive effects of adipogenesis-inducing culture medium on orbital fibroblast lipogenesis were significantly attenuated by butyrate treatment (Figs. 4B, 4C). Therefore, butyrate inhibits GO orbital fibroblast lipogenesis.

To assess the effects of butyrate on adipogenesis in human-derived healthy orbital fibroblasts, the cells were cultured in adipogenesis-inducing medium in the presence or absence of butyrate (10 µM). Lipid droplet formation was significantly enhanced by adipogenesis-inducing medium, as shown by Oil-Red O staining (Fig. 5A), whereas butyrate treatment markedly suppressed lipid droplet accumulation. Furthermore, the adipogenesis-inducing medium significantly increased the protein levels and mRNA expression of c/EBPα, c/EBPβ, PPARγ, perilipin-1, FABP4, leptin, and adiponectin (Figs. 5B, 5C). Butyrate treatment substantially decreased the expression of these markers, demonstrating its inhibitory effects on adipogenesis in normal orbital fibroblasts. Similarly, butyrate treatment alone caused no significant alterations in healthy orbital fibroblasts.

Butyrate Ameliorates Orbital Histopathological Changes and Thyroid Functions in the GO Mice Model

After exploring the in vitro effects of butyrate, the GO model was established in BALB/c mice and the in vivo effects of butyrate were investigated. Eye appearance observations showed notable signs of orbital pathology, including redness and swelling in the GO model mice, which were partially alleviated by butyrate treatment (Fig. 6A). MRI imaging confirmed an increase in extraocular muscle (EOM) volume and edema in GO model mice compared with healthy controls, whereas butyrate supplementation significantly reduced these changes, as indicated by the EOM measurements (Fig. 6B). Histopathological analysis of orbital tissues further validated these findings. H&E staining revealed enlarged muscle fibers in GO mice, which were partially improved following butyrate treatment (Fig. 6C). Masson staining showed increased collagen deposition in the orbital tissues of GO mice, which was reduced with butyrate supplementation (Fig. 6D). IHC staining for FABP4 indicated an increase in adipose tissue within the GO group, whereas butyrate treatment partially decreased adipose tissue levels (Fig. 6E). Similarly, IHC staining for α-SMA, a marker of myofibroblast activation, showed elevated level in GO mice, which was also partially reduced by butyrate treatment (Fig. 6F). Quantitative analysis revealed that the relative collagen area and adipose tissue area were significantly increased in GO mice compared with the healthy controls, with both parameters showing partial reductions following butyrate treatment (Figs. 6G, 6H). These results suggest that butyrate treatment alleviates orbital histopathological alterations, including muscle fibrosis and adipose tissue expansion, in the GO mouse model.

Regarding thyroid functions, the body weight of the mice from all groups was measured on weeks 0, 3, 6, 9, 12, and 15 of modeling; Figure 7A shows no obvious changes in the body weight of mice from the GO and butyrate treatment groups. Histopathological alterations in mice thyroid tissues were examined using H&E staining; the morphology of GO model mice exhibited typical hyperplastic changes, which was partially ameliorated by butyrate (Fig. 7B). Serum levels of T4, TSAb, TSBAb, T3, FT4, and TSH in mice from different groups were determined using corresponding ELISA kits. Figure 7C shows that the serum levels of T4, TSAb, TSBAb, T3, and FT4 were significantly increased, whereas TSH was reduced in the GO model mice compared with the healthy controls; butyrate treatment remarkably decreased T4, TSAb, TSBAb, T3, and FT4 serum levels but increased TSH levels in the GO model mice. Regarding the fibrotic and adipogenic markers, vimentin, fibronectin, collagen I, collagen III, α-SMA, c/EBPα, c/EBPβ, PPARγ, perilipin-1, FABP4, leptin, and adiponectin protein contents were dramatically increased in orbital tissues from GO model mice, whereas partially decreased by butyrate treatment (Figs. 7D, 7E). These findings indicate that butyrate could improve the orbital histopathological alterations and thyroid functions in the GO model mice.

Butyrate Alters the Gut Microbiota Diversity in the GO Model Mice

Because the intestinal microbiota might be influenced by metabolites, fecal samples were collected from mice in different groups and subjected to 16S rDNA sequencing to analyze the diversity of the microbiota community. Faith_pd, Chao1, ACE, Goods_coverage, Simpson, and Observed were applied to evaluate the α-diversity; Figure 8A shows no remarkable between-sample variation in the diversity of gut microbiota from each group. The between-group variations in the microbial community were assessed by conducting Beta diversity analysis with Anosim. Figure 8B shows that the R value is 0.515 (>0), suggesting that dissimilarities are greater between groups than within groups; the P value was 0.001 (<0.05), indicating statistical significance. PCA analysis was performed to identify the principal component and further examine the between-group variations in the gut microbial community; Figure 8C shows that samples were well separated among the groups. The OTUs were annotated within groups and overlapping OTUs among groups were shown in the Venn diagram. Figure 8D shows that a total of 540 overlapping OTUs were identified.

Next, the relative abundance of dominant species was analyzed. Kruskal-Wallis analysis was performed to select the different bacteria among the groups, and the different bacteria at genus levels were classified in accordance with the relative abundance. The top 10 bacteria are shown in Figures 9A and 9B and the Table. The abundance of *Bifidobacterium*, *GCA-900066575*, and *Parabacteroides* showed to be remarkably decreased within the GO mice than normal controls (Fig. 9C). The abundance of *Colidextribacter*, *Desulfovibrio*, *Oscillibacter*, and *Roseburia* tended to decrease but the differences were insignificant (see Fig. 9C). The abundance of the *Bacteroides* and *Erysipelatoclostridium* tended to elevate in GO mice but the difference was insignificant (see Fig. 9C). The abundance of *Bacteroides* and *Rikenellaceae_RC9_gut_group* showed to be dramatically higher within the GO + butyrate mice than the GO mice (see Fig. 9C). *GCA-900066575* and *Parabacteroides* abundance tended to be higher within the GO + butyrate mice but the difference showed to be insignificant (Fig. 9C). The abundance of *Bifidobacterium*, *Colidextribacter*, *Desulfovibrio*, *Oscillibacter*, and *Roseburia* had a decreasing trend in abundance in GO + butyrate compared with GO mice, but the difference was insignificant (see Fig. 9C). Moreover, GO-induced downregulation of *GCA-*

Investigative Ophthalmology & Visual Science

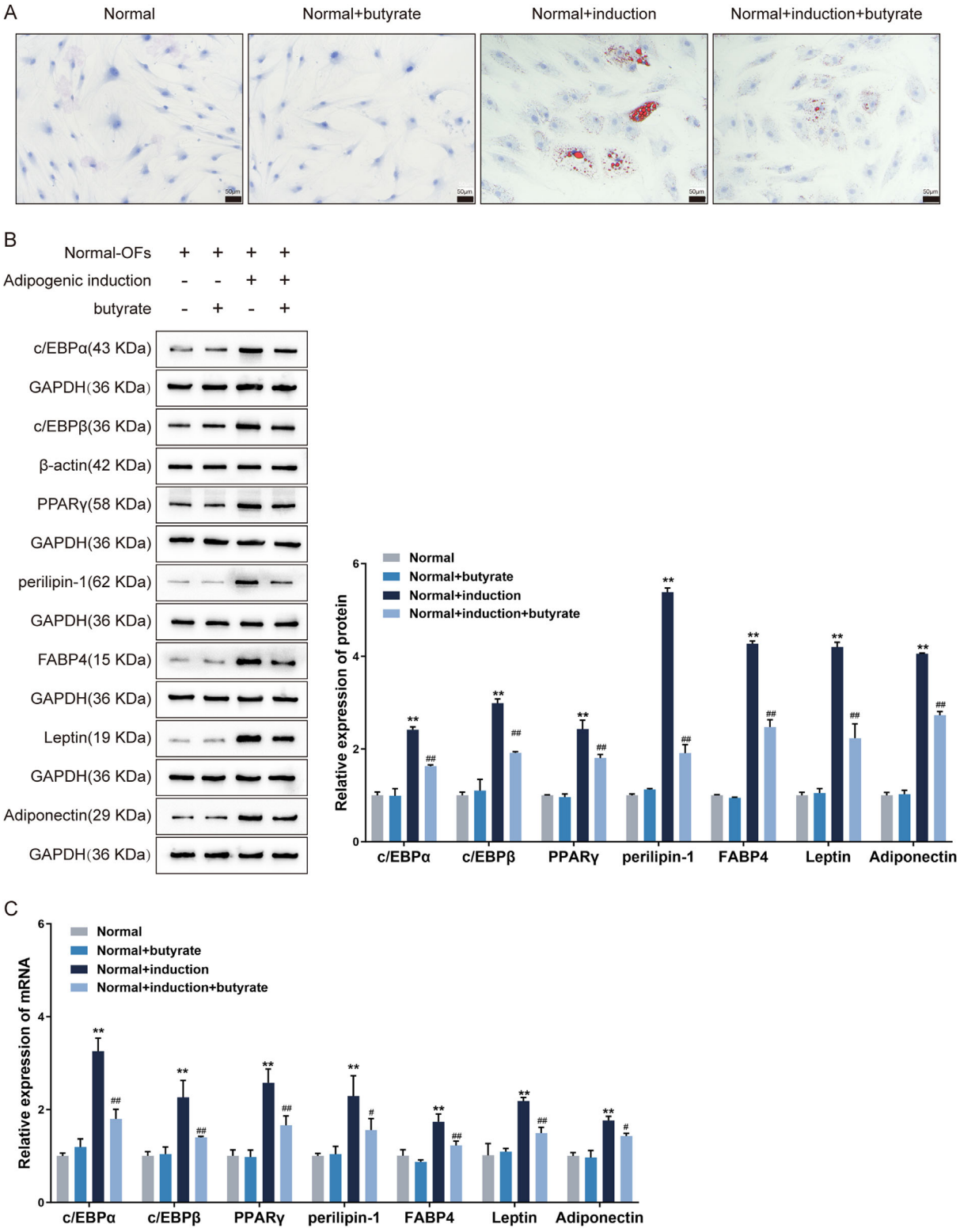

Figure 5. Effects of butyrate on healthy orbital fibroblast adipogenesis. Healthy orbital fibroblasts were cultivated in standard or adipogenesis-inducing culture medium, with or without butyrate (10 μM), and examined for lipid droplet formation using Oil-Red O staining (induction for 10 days) (**A**); the protein levels of c/EBPα, c/EBPβ, PPARγ, perilipin-1, FABP4, leptin, and adiponectin using immunoblotting (**B**); the mRNA expression levels of c/EBPα, c/EBPβ, PPARγ, perilipin-1, FABP4, leptin, and adiponectin using qRT-PCR (**C**) (induction for 4 days, $n = 3$, $^{**}P < 0.01$ vs. the healthy group; $^{\#\#}P < 0.01$ vs. the healthy + induction group).

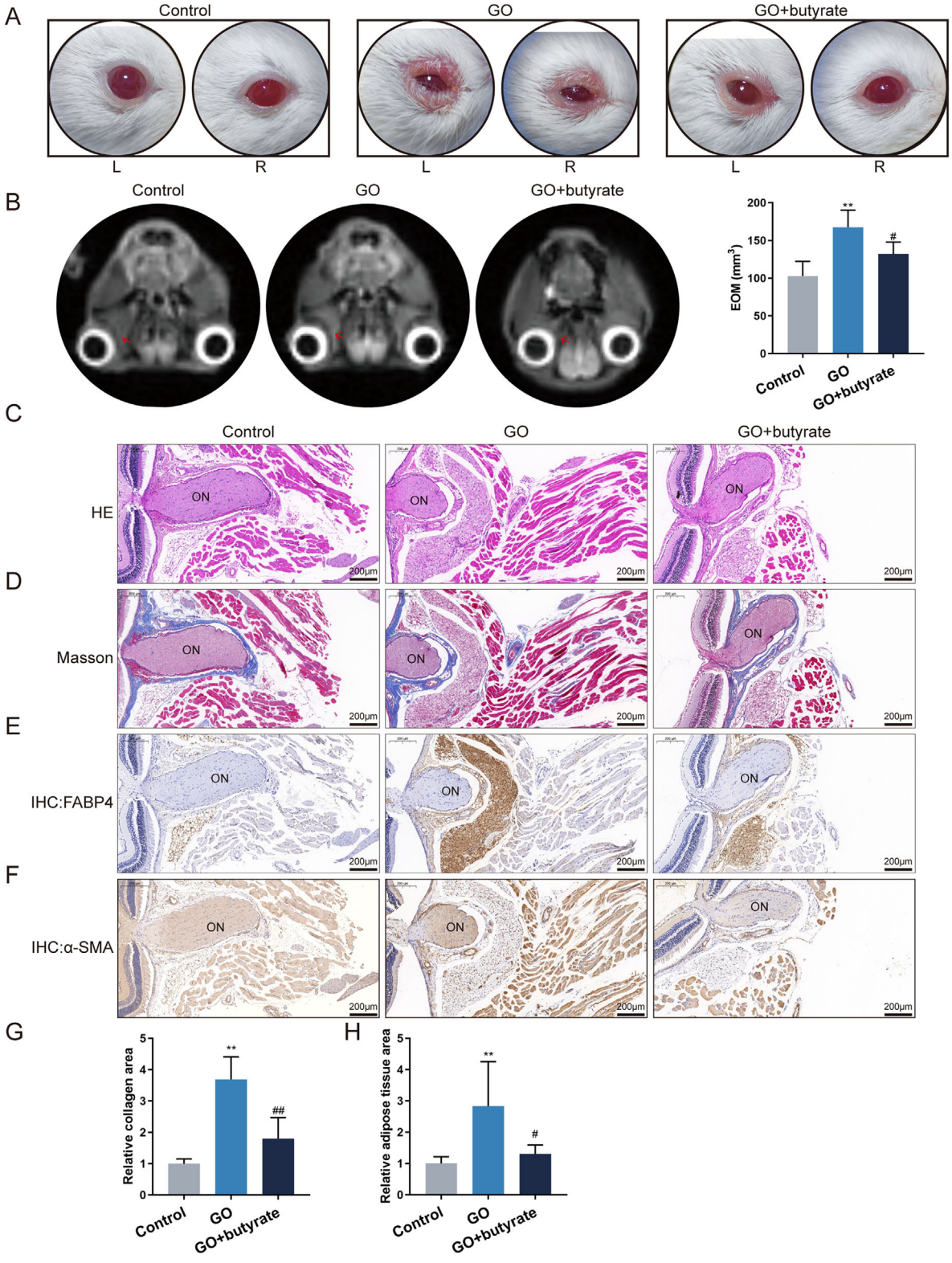

Figure 6. Butyrate relieves orbital histopathological changes in the GO mice model. BALB/c mice were immunized with the Ad-TSHR for GO model establishment, with or without butyrate; at the end of modeling, the mice from different groups were examined for mice eye appearance (**A**); orbit and extraocular muscle (*red arrows* indicated) was observed using MRI scanning (**B**); histopathological alterations in orbital tissues were examined using H&E staining (**C**); histopathological alterations in orbital muscular tissues were examined using Masson staining (**D**); IHC staining of α-SMA and FABP4 levels (**E**); relative collagen and adipose tissue area were calculated according to histopathological evaluation ($n = 6$, $^{**}P < 0.01$ vs. the control group; $^{\#}P < 0.05$, $^{\#\#}P < 0.01$ vs. the GO group).

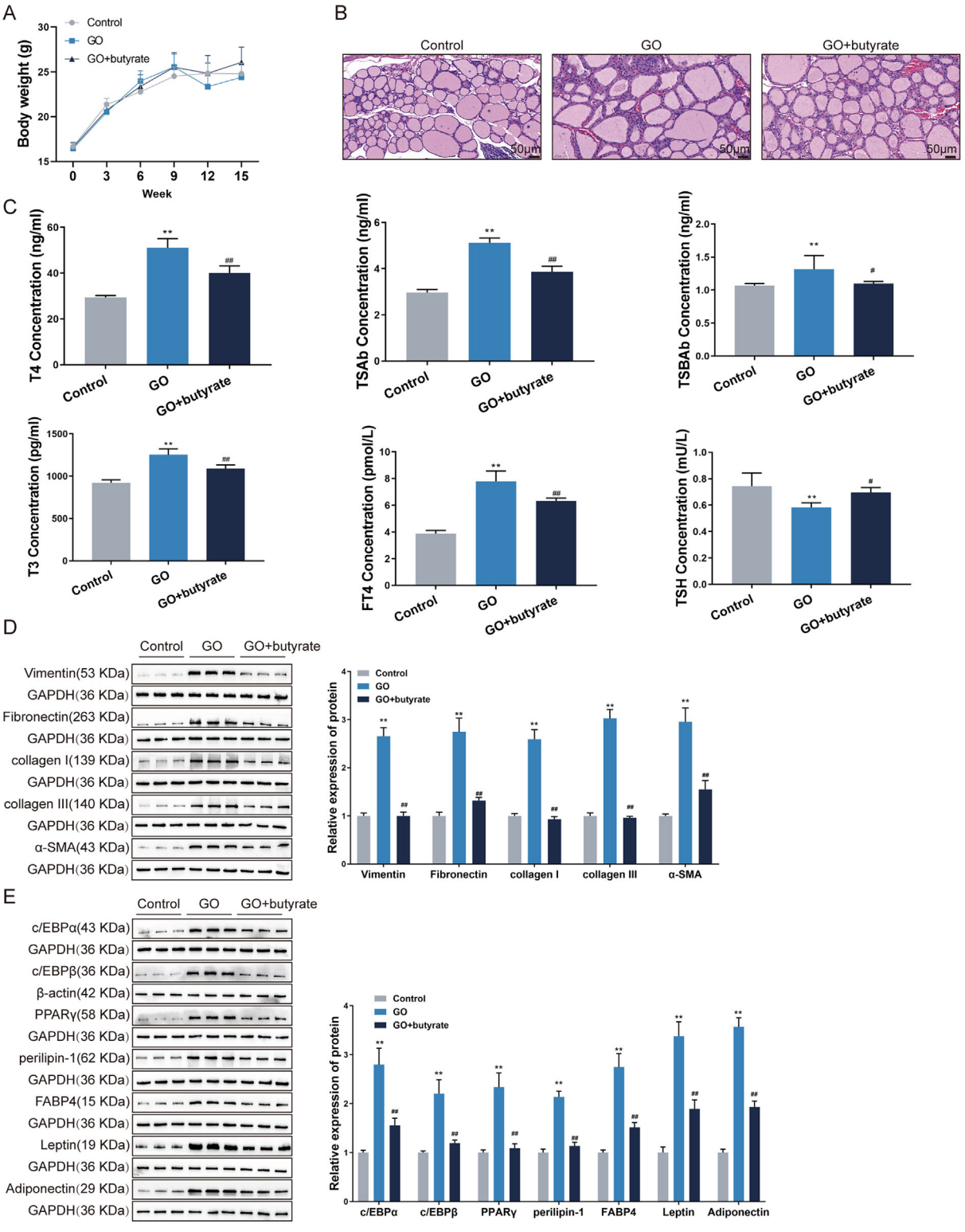

Figure 7. Butyrate ameliorates thyroid functions in the GO mice model. (**A**) Body weight of mice in each group was measured on weeks 0, 3, 6, 9, 12, and 15 of modeling. (**B**) Histopathological alterations in mice thyroid tissues were examined using H&E staining. (**C**) Serum levels of T4, TSAb, TSBAb, T3, FT4, and TSH in mice from different groups were determined using corresponding ELISA kits ($n = 6$). (**D, E**) The protein levels of vimentin, fibronectin, collagen I, collagen III, α-SMA, c/EBPα, c/EBPβ, PPARγ, perilipin-1, FABP4, leptin, and adiponectin in orbital tissues were examined using Immunoblotting ($n = 3$, $^{**}P < 0.01$ vs. the healthy control group; $^{\#}P < 0.05$, $^{\#\#}P < 0.01$ vs. the GO group).

Investigative Ophthalmology & Visual Science

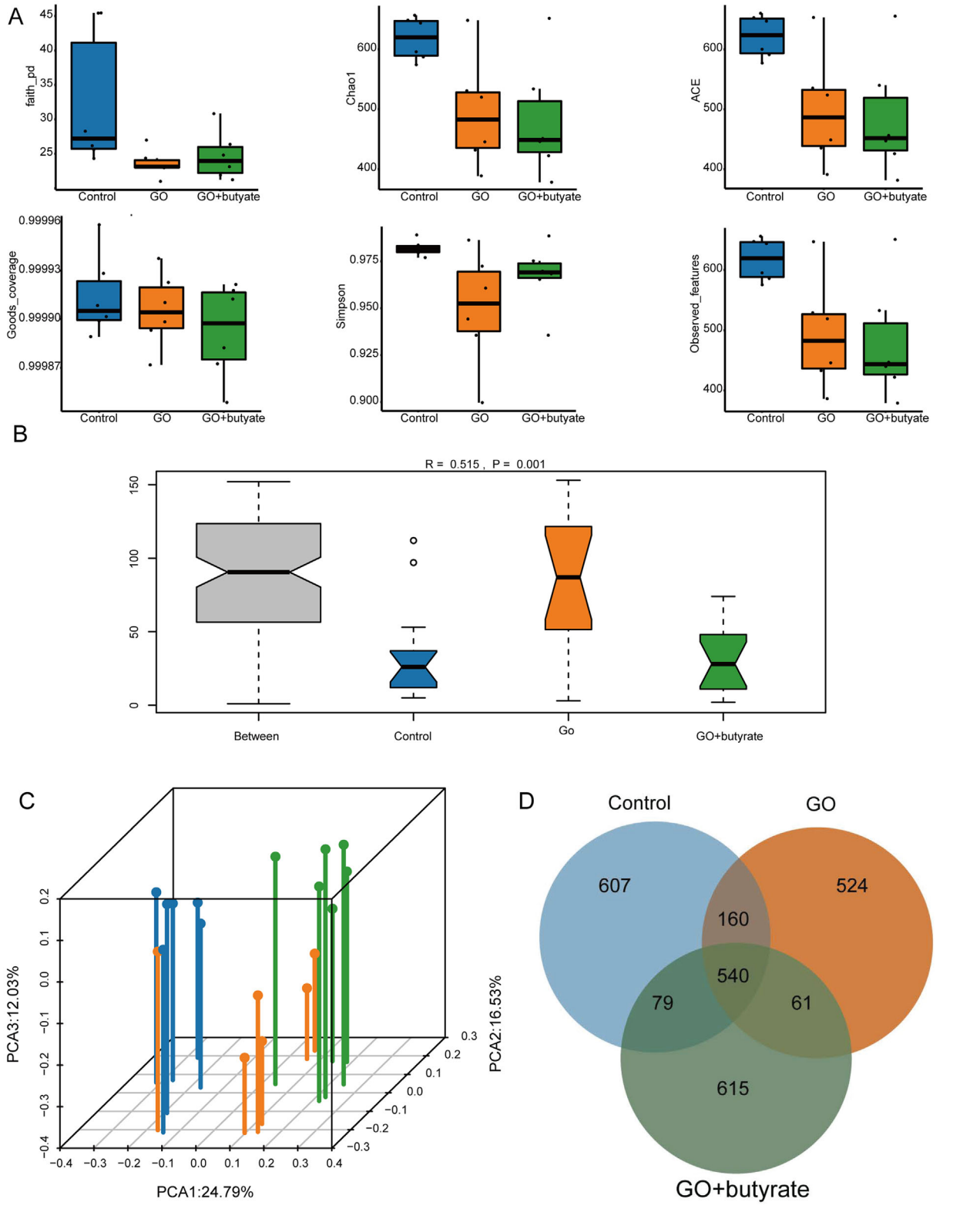

Figure 8. Butyrate alters the diversity of gut microbiota in the GO model mice. Fecal samples were collected from mice in different groups and applied for 16S rDNA sequencing for microbial community diversity analysis. (**A**) The α-diversity was evaluated using Faith_pd, Chao1, ACE, Goods_coverage, Simpson, and Observed. (**B**) The β-diversity was evaluated using Anosim. (**C**) PCA analysis was performed to evaluate the difference in the gut microbial community among the different groups. (**D**) Annotated operational taxonomic units (OTUs) within groups and overlapping among groups were shown in the Venn diagram ($n = 6$).

Investigative Ophthalmology & Visual Science

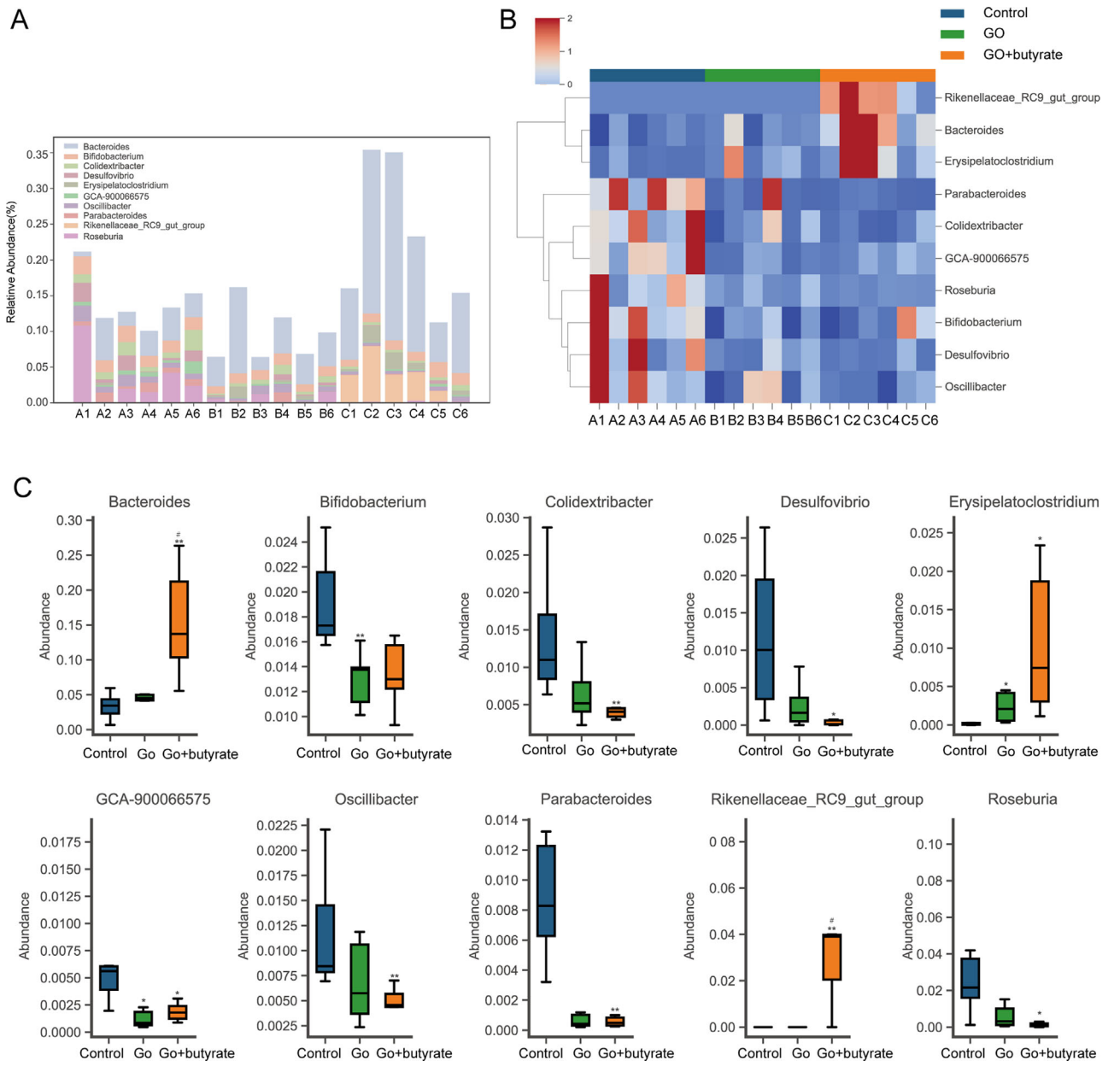

Figure 9. Butyrate alters the relative abundance of dominant species at the genus level. (**A**) Kruskal-Wallis analysis was performed to select the different bacteria among the groups, and the different bacteria were sorted according to the relative abundance; the top 10 bacteria were shown. (**B**) Hierarchical clustering heatmap showing the top 10 bacteria. (**C**) The relative abundance of the top 10 bacteria ($n = 6$, $^{*}P < 0.05$, $^{**}P < 0.01$ vs. the healthy control group; $^{\#}P < 0.05$ vs. the GO group).

Table. Top 10 Differential Bacteria Among the Groups According to Relative Abundance

Gut	*P* Value	GO Vs. Control Groups	GO Vs. The GO + Butyrate Group
Bacteroides	0.007707996	Up	Down*
Bifidobacterium	0.024109575	Down*	Up
Colidextribacter	0.014752035	Down	Up
Desulfovibrio	0.033677467	Down	Up
Erysipelatoclostridium	0.009468549	Up	Down
GCA-900066575	0.00871517	Down*	Down
Oscillibacter	0.038717562	Down	Up
Parabacteroides	0.018315639	Down*	Down
Rikenellaceae_RC9_gut_group	0.004075319	–	Down*
Roseburia	0.038717562	Down	Up

* Indicated $P < 0.05$ between two groups.

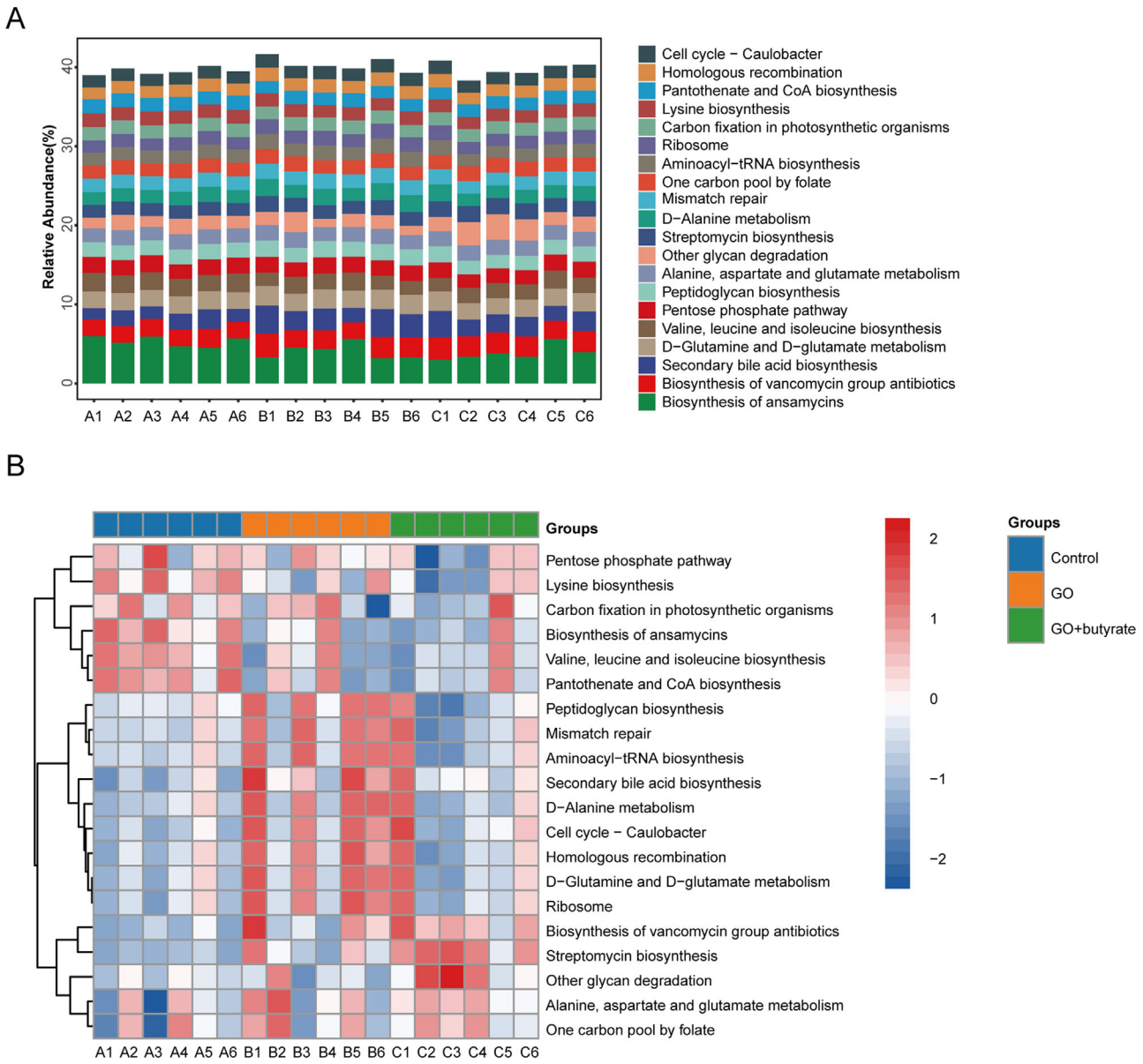

Figure 10. Metabolic functions of gut microbiota predicted using PICRUSt2. Available at: https://github.com/picrust/picrust2.

900066575 and *Parabacteroides* abundance were increased by butyrate supplementation.

Last, using PICRUSt2 (https://github.com/picrust/picrust2),[50] the gene function profiles of the common ancestors of microorganisms were inferred on the basis of the full-length 16S rRNA sequences of their genomes, and gene function prediction profiles were constructed for the entire spectrum of archaeal and bacterial domains. Finally, the composition of the sequenced colonies was "mapped" to the KEGG gene database to predict the effects of the bacteria. As shown in Figures 10A and 10B, the metabolic functions of the bacteria were primarily associated with antimycotic biosynthesis, vancomycin antibiotic biosynthesis, secondary bile acid biosynthesis, D-glutamine and D-glutamic acid metabolism, valine, leucine, and isoleucine biosynthesis, pentose phosphate pathway, peptidoglycan biosynthesis, alanine, aspartic acid, and glutamic acid metabolism, degradation of other glycans, streptomycin biosynthesis, d-alanine metabolism, mismatch repair, folate carbon pool, the Aminoacyl-trna biosynthesis, ribosomes, carbon fixation in photosynthetic organisms, lysine biosynthesis, pantothenic acid and coenzyme a biosynthesis, homologous recombination, cell cycle-caulobacter, and other functions. Among those metabolic pathways, cell cycle-caulobacter, ribosome, secondary bile acid biosynthesis, D-glutamine and D-glutamate metabolism and homologous recombination levels were increased, valine, leucine and isoleucine biosynthesis, and pantothenate and CoA biosynthesis levels were decreased in GO mice ($P < 0.05$), but butyrate supplementation did not significantly alter these changes ($P > 0.05$; Fig. 11).

Discussion

Herein, the effects of butyrate upon GO were investigated, focusing on its impact on orbital fibroblast cell viabil-

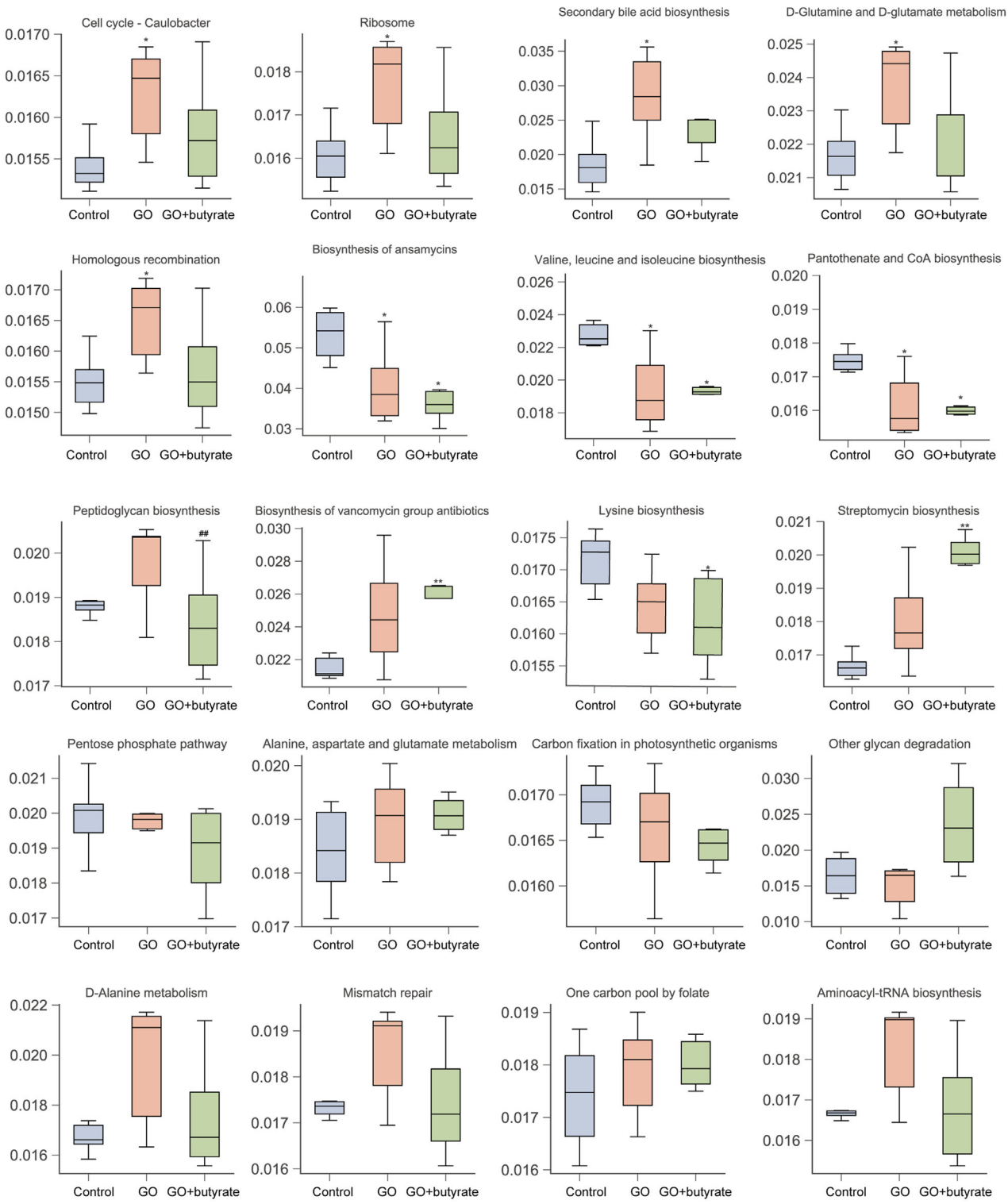

Figure 11. The difference of predicted metabolic functions of gut microbiota in the healthy control, the GO, and the GO + butyrate mice. ($n = 6$, $^{*}P < 0.05$, $^{**}P < 0.01$ vs. the healthy group; $^{\#\#}P < 0.01$ vs. the GO group).

ity, activation, and adipogenesis, and its in vivo effects on a GO mouse model and on gut microbiota diversity. Butyrate significantly inhibited the viability of GO orbital fibroblasts, whereas having no detrimental effects on normal fibroblasts. Additionally, TGF-β1-induced activation and fibrotic processes in healthy and GO fibroblasts were suppressed by butyrate, as evidenced by decreased protein and mRNA levels of various fibroblast activation markers. In terms of adipogenesis, butyrate was found to reduce lipid droplet formation and downregulate key lipogenic mark-

ers in GO and healthy orbital fibroblasts. In the GO mouse model, butyrate treatment led to improvements in orbital histopathological changes, including a reduction in muscle thickness, edema, muscle fiber enlargement, and collagen deposition. Furthermore, serum thyroid hormone and antibody levels were normalized in these mice, indicating a positive influence on thyroid functions. In terms of gut microbiota, significant alterations were noted in the composition of the GO model mice treated with butyrate. Specifically, there was a shift in the microbial community diversity and abundance, with a decreased abundance of *Bifidobacterium*, *GCA-900066575*, and *Parabacteroides* in the GO group compared with control mice, and increased abundance of *Bacteroides* and *Rikenellaceae_RC9* in the GO + butyrate group compared with GO mice. These findings indicate that butyrate has a multifaceted role in modulating thyroid-related pathologies and altering the gut microbiota, providing important insights into the gut-thyroid axis in GO.

Based on GO, the role of butyrate in regulating orbital fibroblast proliferation, fibrosis, and adipogenesis is particularly noteworthy given the critical influence of orbital fibroblasts in GO pathology.[6,51] During GO's active stage, these fibroblasts undergo marked proliferation and adipogenesis, secreting inflammatory mediators and hyaluronan essential for tissue remodeling.[52] Our study reveals that butyrate selectively inhibits GO orbital fibroblasts' viability without impacting normal ones, especially at higher doses and over prolonged periods. This underscores butyrate's potential in specifically targeting GO's pathological processes without compromising normal fibroblast functions. More importantly, butyrate also attenuated TGF-β1-induced activation of normal orbital fibroblast without causing any cytotoxicity while applying alone. Additionally, butyrate effectively reduces lipid droplet formation in both GO and healthy orbital fibroblasts, a key aspect of adipogenesis in GO.[53,54] Butyrate also downregulates critical adipogenesis markers, including c/EBPα, c/EBPβ, PPARγ, perilipin-1, FABP4, leptin, and adiponectin. These markers, involved in adipocyte differentiation and lipid metabolism, are modulated by PPARγ activators, with leptin and adiponectin exclusively produced by mature adipocytes and linked to metabolic activities like insulin sensitivity and anti atherogenesis properties.[55–60] Thus, butyrate's inhibitory effect on these markers indicates its role in curbing GO orbital fibroblast lipogenesis. Furthermore, the improvement of healthy orbital fibroblast activation and adipogenesis by butyrate indicates that butyrate's actions are not exclusive to GO fibroblasts but may represent a broader mechanism of action in orbital fibroblast biology.

During the inactive stage of GO, chronic fibrosis, characterized by persistent hyaluronan deposition and adipogenesis, becomes dominant.[61,62] This ongoing activity of orbital fibroblasts fuels the disease's progression, highlighting their importance as targets for novel therapies like monoclonal antibodies and small molecular antagonists directed at the TSHR.[63–65] Under this context, butyrate shows notable effects in regulating orbital fibroblasts. It suppresses both the proliferation and migration of GO orbital fibroblasts, even in standard culture media. This effect is particularly evident when TGF-β1 is present, a known stimulator of GO orbital fibroblast proliferation and migration.[66] During fibrosis, characterized by unchecked fibroblast proliferation, migration, transformation into α-SMA-producing myofibroblasts, and accumulation of extracellular matrix components such as collagen and fibronectin,[67] butyrate's impact is significant. Our study found that butyrate suppresses these fibrotic processes and downregulates fibroblast activation markers, such as vimentin,[68] fibronectin,[69] collagen I and III, and α-SMA. This suggests butyrate's role in mitigating TGF-β1-triggered GO orbital fibroblast activation and fibrosis.

Following the verification of butyrate's in vitro effects on orbital fibroblasts, its in vivo role was explored in a GO model using BALB/c mice, demonstrating significant improvement in both orbital histopathological changes and thyroid functions. The study observed the main histopathological features of GO, such as increased orbital muscle thickness, edema, enlarged muscle fibers, and enhanced orbital collagen deposition,[70] all of which were notably ameliorated by butyrate treatment. Additionally, butyrate partially alleviated the observed fat expansion in GO model mice.[71] Concerning thyroid function, no significant body weight changes were detected among the groups, but histopathological examination of thyroid tissues revealed hyperplastic changes in the GO model mice, which were partially reduced by butyrate. Serum analysis further supported these findings, showing butyrate effectively normalized the altered levels of T4, TSAb, TSBAb, T3, FT4, and TSH typically observed in GO mice. As previously reported, male and female mice were induced to develop hyperthyroidism by immunization with human TSHR A-subunit encoding plasmids, marked by TSHR-stimulating antibodies, increased T4 levels, thyroid gland pathology, and cardiac hypertrophy.[43] Moreover, TSAb and TSBAb showed to be extensively distributed and persistent in mice immunized by Ad-TSHR over seven immunizations, supporting the effective creation of a long-term murine model for GD.[72] Moreover, the protein levels of fibrotic and adipogenic markers markedly elevated within the orbital tissue samples of GO model mice were partially decreased following butyrate treatment. Collectively, these findings highlight butyrate's substantial potential in improving orbital histopathological alterations and thyroid functions in the GO model mice.

The study's analysis of gut microbiota diversity and dominant species abundance highlighted the impact of butyrate on gut microbiota composition. Although α-diversity revealed no significant differences across the groups, β-diversity analysis underscored distinct variations, indicating butyrate's influence. Notably, within the GO group, there was a remarkable decrease in *Bifidobacterium*, *GCA-900066575*, and *Parabacteroides* than the healthy group. Nevertheless, butyrate treatment induced a remarkable reduction in the abundance of *Bacteroides* and *Rikenellaceae_RC9* compared with the GO group. *Bifidobacterium*, a probiotic, has been noted to decrease in autoimmune thyroid diseases,[73] and its supplementation alongside methimazole improved thyroid function in patients with GD through the gut-thyroid axis.[74] Similar to our finding, a reduction of *Parabacteroides* abundance has been reported in patients with GD[75] and rat models of hyperthyroidism.[76] *Rikenellaceae_RC9*, linked to adipocyte signaling,[77] is known for promoting fat digestion and absorption[78] and inversely correlates with FT3 and FT4 levels.[79] *GCA-900066575*, on the other hand, exhibits multifaceted roles. In high-fat diet-fed mice, it positively correlated with various metabolic indicators,[80] whereas an anti-lipid agent (TF3) increased its abundance.[81] Considering the association of *Rikenellaceae_RC9* and *GCA-900066575* with adipogenesis and lipid metabolism, these two species might mediate the effects of butyrate in improving orbital fibroblast adipogen-

Investigative Ophthalmology & Visual Science

esis and activation, as well as GO mice orbital histopathological alterations and thyroid functions.

Previous serum metabolomic analysis in patients with GD found that hyperthyroidism had higher levels of glutamine.[82] Increasing serum glutamine levels are associated with thyroid autoimmunity.[83] Lee et al.[84] demonstrated that valine, leucine, and isoleucine biosynthesis differed before and after methimazole treatment in patients with GD. In the present study, the metabolic function's prediction of gut microbiota also found that glutamine and glutamate metabolism and valine, leucine, and isoleucine biosynthesis are altered in GO mice and reversed by butyrate supplementation. The potential role of butyrate in the regulation of those pathways in GO needs further investigation. Butyrate, a short-chain fatty acid derived from gut microbiota, exerts multifaceted effects that could account for its therapeutic potential in GO. One of its well-known mechanisms is the inhibition of histone deacetylases (HDACs),[85] which leads to the regulation of gene expression involved in inflammation and fibrosis.[86–88] Through HDAC inhibition, butyrate suppresses proinflammatory cytokine production and fibroblast activation, as demonstrated by its downregulation of TGF-β1-induced activation markers. Additionally, butyrate influences adipogenesis by modulating PPARγ signaling, thereby reducing lipid droplet formation and the expression of adipogenic markers. Beyond its local effects on fibroblasts, butyrate also contributes to systemic regulation by modulating gut microbiota composition. The observed increase in beneficial bacteria such as *Bacteroides* and *Rikenellaceae_RC9* suggests that butyrate helps restore gut microbial balance, which might impact immune system regulation via the gut-thyroid axis. Furthermore, the anti-inflammatory properties of butyrate, such as its suppression of NF-κB signaling,[89] and its ability to promote mitochondrial[90] function could enhance cellular homeostasis in GO. These collective effects provide a mechanistic framework to explain how butyrate ameliorates GO pathology, from reducing fibrosis and adipogenesis to restoring immune and metabolic balance.

The ex vivo assays using human orbital fibroblasts highlight the direct cellular effects of butyrate on fibroblast activation and adipogenesis, offering insight into its potential mechanisms in human GO pathology. These findings are complemented by the in vivo data from the GO mouse model, which provide evidence of the systemic effects of butyrate, including gut microbiota modulation and thyroid hormone regulation. Although murine models have limitations in translatability to human disease, the inclusion of human ex vivo tissues strengthens the relevance of our findings. Future studies should focus on clinical trials to confirm the efficacy of butyrate in human patients and explore its potential integration into current GO management strategies.

Conclusions

In conclusion, this study highlights butyrate's significant role in managing GO by modulating orbital fibroblast activity and altering gut microbiota. Its ability to selectively inhibit GO orbital fibroblast viability and adipogenesis and suppress TGF-β1-induced fibrosis, without impacting normal fibroblasts, demonstrates its targeted therapeutic potential. Additionally, butyrate normalizes thyroid function in a GO mouse model, improves histopathological alterations, and modulates specific gut microbiota populations, underscoring its effectiveness in treating thyroid-related pathologies and providing insights into the gut-thyroid axis in GO management.

Acknowledgments

Supported by the Natural Science Foundation of Hunan Province (2023JJ20085), the National Nature Science Foundation of China (82301264), and the Science and Technology Innovation Program of Hunan Province (2023RC3084).

Availability of Data and Materials: The data supporting this study's findings are available from the corresponding author upon reasonable request.

Author Contributions: P.B., O.Y., and J.Q. performed the experiments and wrote the main manuscript text. B.D.T., Y.P.L., and J.M.C. performed the experiments. L.J.W, and T.X.N. coordinated the study and assisted with the experiments. X.Q. guided the experiment and plan, conceived the study, designed the experiments, and revised the paper. All the authors have reviewed and approved the manuscript.

Disclosure: **P. Ouyang**, None; **J. Qi**, None; **B. Tong**, None; **Y. Li**, None; **J. Cao**, None; **L. Wang**, None**; T. Niu**, None; **X. Qi**, None

References

1. Reddy SV, Jain A, Yadav SB, Sharma K, Bhatia E. Prevalence of Graves' ophthalmopathy in patients with Graves' disease presenting to a referral centre in north India. *Indian J Med Res*. 2014;139(1):99–104.
2. Tellez M, Cooper J, Edmonds C. Graves' ophthalmopathy in relation to cigarette smoking and ethnic origin. *Clin Endocrinol (Oxf)*. 1992;36(3):291–294.
3. Wiersinga WM, Bartalena L. Epidemiology and prevention of Graves' ophthalmopathy. *Thyroid*. 2002;12(10):855–860.
4. Tanda ML, Piantanida E, Liparulo L, et al. Prevalence and natural history of Graves' orbitopathy in a large series of patients with newly diagnosed graves' hyperthyroidism seen at a single center. *J Clin Endocrinol Metab*. 2013;98(4):1443–1449.
5. Draman MS, Zhang L, Dayan C, Ludgate M. Orbital signaling in Graves' orbitopathy. *Front Endocrinol (Lausanne)*. 2021;12:739994.
6. Dik WA, Virakul S, van Steensel L. Current perspectives on the role of orbital fibroblasts in the pathogenesis of Graves' ophthalmopathy. *Exp Eye Res*. 2016;142:83–91.
7. Marino M, Rotondo Dottore G, Ionni I, et al. Serum antibodies against the insulin-like growth factor-1 receptor (IGF-1R) in Graves' disease and Graves' orbitopathy. *J Endocrinol Invest*. 2019;42(4):471–480.
8. Perros P, Hegedus L, Bartalena L, et al. Graves' orbitopathy as a rare disease in Europe: a European Group on Graves' Orbitopathy (EUGOGO) position statement. *Orphanet J Rare Dis*. 2017;12(1):72.
9. Taylor PN, Zhang L, Lee RWJ, et al. New insights into the pathogenesis and nonsurgical management of Graves orbitopathy. *Nat Rev Endocrinol*. 2020;16(2):104–116.
10. Wiersinga WM. Advances in treatment of active, moderate-to-severe Graves' ophthalmopathy. *Lancet Diabetes Endocrinol*. 2017;5(2):134–142.
11. Weetman AP. Immunity, thyroid function and pregnancy: molecular mechanisms. *Nat Rev Endocrinol*. 2010;6(6):311–318.
12. Wiesweg B, Johnson KT, Eckstein AK, Berchner-Pfannschmidt U. Current insights into animal models

of Graves' disease and orbitopathy. *Horm Metab Res*. 2013;45(8):549–555.
13. Bagnasco M, Bossert I, Pesce G. Stress and autoimmune thyroid diseases. *Neuroimmunomodulation*. 2006;13(5–6):309–317.
14. Eckstein A, Quadbeck B, Mueller G, et al. Impact of smoking on the response to treatment of thyroid associated ophthalmopathy. *Br J Ophthalmol*. 2003;87(6):773–776.
15. Antonelli A, Fallahi P, Elia G, et al. Graves' disease: Clinical manifestations, immune pathogenesis (cytokines and chemokines) and therapy. *Best Pract Res Clin Endocrinol Metab*. 2020;34(1):101388.
16. Antonelli A, Ferrari SM, Ragusa F, et al. Graves' disease: Epidemiology, genetic and environmental risk factors and viruses. *Best Pract Res Clin Endocrinol Metab*. 2020;34(1):101387.
17. Saini A, Dalal P, Sharma D. Deciphering the interdependent labyrinth between gut microbiota and the immune system. *Lett Appl Microbiol*. 2022;75(5):1122–1135.
18. Maslowski KM, Mackay CR. Diet, gut microbiota and immune responses. *Nat Immunol*. 2011;12(1):5–9.
19. Honda K, Littman DR. The microbiota in adaptive immune homeostasis and disease. *Nature*. 2016;535(7610):75–84.
20. Hooper LV, Macpherson AJ. Immune adaptations that maintain homeostasis with the intestinal microbiota. *Nat Rev Immunol*. 2010;10(3):159–169.
21. Hooper LV, Littman DR, Macpherson AJ. Interactions between the microbiota and the immune system. *Science*. 2012;336(6086):1268–1273.
22. Masetti G, Moshkelgosha S, Kohling HL, et al. Gut microbiota in experimental murine model of Graves' orbitopathy established in different environments may modulate clinical presentation of disease. *Microbiome*. 2018;6(1):97.
23. Li Y, Luo B, Tong B, et al. The role and molecular mechanism of gut microbiota in Graves' orbitopathy. *J Endocrinol Invest*. 2023;46(2):305–317.
24. Moshkelgosha S, Masetti G, Berchner-Pfannschmidt U, et al. Gut microbiome in BALB/c and C57BL/6J mice undergoing experimental thyroid autoimmunity associate with differences in immunological responses and thyroid function. *Horm Metab Res*. 2018;50(12):932–941.
25. Moshkelgosha S, Verhasselt HL, Masetti G, et al. Modulating gut microbiota in a mouse model of Graves' orbitopathy and its impact on induced disease. *Microbiome*. 2021;9(1):45.
26. Vitale G, Dicitore A, Barrea L, et al. From microbiota toward gastro-enteropancreatic neuroendocrine neoplasms: are we on the highway to hell? *Rev Endocr Metab Disord*. 2021;22(3):511–525.
27. Lv LX, Fang DQ, Shi D, et al. Alterations and correlations of the gut microbiome, metabolism and immunity in patients with primary biliary cirrhosis. *Environ Microbiol*. 2016;18(7):2272–2286.
28. Jiang W, Lu G, Qiao T, et al. Integrated microbiome and metabolome analysis reveals a distinct microbial and metabolic signature in Graves' disease and hypothyroidism. *Heliyon*. 2023;9(11):e21463.
29. De Filippis F, Pasolli E, Ercolini D. Newly explored faecalibacterium diversity is connected to age, lifestyle, geography, and disease. *Curr Biol*. 2020;30(24):4932–4943.e4.
30. Quevrain E, Maubert MA, Michon C, et al. Identification of an anti-inflammatory protein from Faecalibacterium prausnitzii, a commensal bacterium deficient in Crohn's disease. *Gut*. 2016;65(3):415–425.
31. Zhang M, Qiu X, Zhang H, et al. Faecalibacterium prausnitzii inhibits interleukin-17 to ameliorate colorectal colitis in rats. *PLoS One*. 2014;9(10):e109146.
32. Zhang Q, Tong B, Xie Z, et al. Changes in the gut microbiota of patients with Graves' orbitopathy according to severity grade. *Clin Exp Ophthalmol*. 2023;51:808–821.
33. Hamer HM, Jonkers DM, Vanhoutvin SA, et al. Effect of butyrate enemas on inflammation and antioxidant status in the colonic mucosa of patients with ulcerative colitis in remission. *Clin Nutr*. 2010;29(6):738–744.
34. Park HJ, Jeong OY, Chun SH, et al. Butyrate improves skin/lung fibrosis and intestinal dysbiosis in bleomycin-induced mouse models. *Int J Mol Sci*. 2021;22(5):2765.
35. Li X, Li R, You N, Zhao X, Li J, Jiang W. Butyric acid ameliorates myocardial fibrosis by regulating M1/M2 polarization of macrophages and promoting recovery of mitochondrial function. *Front Nutr*. 2022;9:875473.
36. Zhao ZH, Wang ZX, Zhou D, et al. Sodium butyrate supplementation inhibits hepatic steatosis by stimulating liver kinase B1 and insulin-induced gene. *Cell Mol Gastroenterol Hepatol*. 2021;12(3):857–871.
37. Wang N, Hou SY, Qi X, et al. LncRNA LPAL2/miR-1287-5p/EGFR axis modulates TED-derived orbital fibroblast activation through cell adhesion factors. *J Clin Endocrinol Metab*. 2021;106(8):e2866–e2886.
38. van Steensel L, Paridaens D, Schrijver B, et al. Imatinib mesylate and AMN107 inhibit PDGF-signaling in orbital fibroblasts: a potential treatment for Graves' ophthalmopathy. *Invest Ophthalmol Vis Sci*. 2009;50(7):3091–3098.
39. Gong Y, Yin JY, Tong BD, Zeng JX, Xiong W. Low density lipoprotein - rosiglitazone - chitosan-calcium alginate/nanoparticles inhibition of human tenon's fibroblasts activation and proliferation. *Oncotarget*. 2017;8(62):105126–105136.
40. Zhou X, Lu J, Wu B, Guo Z. HOXA11-AS facilitates the proliferation, cell cycle process and migration of keloid fibroblasts through sponging miR-188-5p to regulate VEGFA. *J Dermatol Sci*. 2022;106(2):111–118.
41. Xu H, Wang H, Zhao W, et al. SUMO1 modification of methyltransferase-like 3 promotes tumor progression via regulating Snail mRNA homeostasis in hepatocellular carcinoma. *Theranostics*. 2020;10(13):5671–5686.
42. Banga JP, Moshkelgosha S, Berchner-Pfannschmidt U, Eckstein A. Modeling Graves' orbitopathy in experimental Graves' disease. *Horm Metab Res*. 2015;47(10):797–803.
43. Schluter A, Flogel U, Diaz-Cano S. Graves' orbitopathy occurs sex-independently in an autoimmune hyperthyroid mouse model. *Sci Rep*. 2018;8(1):13096.
44. van den Berg FF, van Dalen D, Hyoju SK, et al. Western-type diet influences mortality from necrotising pancreatitis and demonstrates a central role for butyrate. *Gut*. 2021;70(5):915–927.
45. Moshkelgosha S, So PW, Deasy N, Diaz-Cano S, Banga JP. Cutting edge: retrobulbar inflammation, adipogenesis, and acute orbital congestion in a preclinical female mouse model of Graves' orbitopathy induced by thyrotropin receptor plasmid-in vivo electroporation. *Endocrinology*. 2013;154(9):3008–3015.
46. Zhao SX, Tsui S, Cheung A, Douglas RS, Smith TJ, Banga JP. Orbital fibrosis in a mouse model of Graves' disease induced by genetic immunization of thyrotropin receptor cDNA. *J Endocrinol*. 2011;210(3):369–377.
47. Ly A, Buck A, Balluff B, et al. High-mass-resolution MALDI mass spectrometry imaging of metabolites from formalin-fixed paraffin-embedded tissue. *Nat Protoc*. 2016;11(8):1428–1443.
48. Fan J, Wang L, Yang T, et al. Comparative analysis of gut microbiota in incident and prevalent peritoneal dialysis patients with peritoneal fibrosis, correlations with peritoneal equilibration test data in the peritoneal fibrosis

Investigative Ophthalmology & Visual Science

cohort [published online ahead of print November 9, 2024]. *Therc Apher Dial*, doi:10.1111/1744-9987.14226.
49. Langille MG, Zaneveld J, Caporaso JG, et al. Predictive functional profiling of microbial communities using 16S rRNA marker gene sequences. *Nat Biotechnol*. 2013;31(9):814–821.
50. Douglas GM, Maffei VJ, Zaneveld JR, et al. PICRUSt2 for prediction of metagenome functions. *Nat Biotechnol*. 2020;38(6):685–688.
51. Longo CM, Higgins PJ. Molecular biomarkers of Graves' ophthalmopathy. *Exp Mol Pathol*. 2019;106:1–6.
52. Meyer zu Horste M, Stroher E, Berchner-Pfannschmidt U, et al. A novel mechanism involved in the pathogenesis of Graves ophthalmopathy (GO): clathrin is a possible targeting molecule for inhibiting local immune response in the orbit. *J Clin Endocrinol Metab*. 2011;96(11):E1727–E1736.
53. Peyster RG, Ginsberg F, Silber JH, Adler LP. Exophthalmos caused by excessive fat: CT volumetric analysis and differential diagnosis. *AJR Am J Roentgenol*. 1986;146(3):459–464.
54. Kumar S, Coenen MJ, Scherer PE, Bahn RS. Evidence for enhanced adipogenesis in the orbits of patients with Graves' ophthalmopathy. *J Clin Endocrinol Metab*. 2004;89(2):930–935.
55. Siersbaek R, Nielsen R, Mandrup S. PPARgamma in adipocyte differentiation and metabolism–novel insights from genome-wide studies. *FEBS Lett*. 2010;584(15):3242–3249.
56. Spiegelman BM, Hu E, Kim JB, Brun R. PPAR gamma and the control of adipogenesis. *Biochimie*. 1997;79(2–3):111–112.
57. Brun RP, Spiegelman BM. PPAR gamma and the molecular control of adipogenesis. *J Endocrinol*. 1997;155(2):217–218.
58. Zhang Y, Proenca R, Maffei M, Barone M, Leopold L, Friedman JM. Positional cloning of the mouse obese gene and its human homologue. *Nature*. 1994;372(6505):425–432.
59. Scherer PE, Williams S, Fogliano M, Baldini G, Lodish HF. A novel serum protein similar to C1q, produced exclusively in adipocytes. *J Biol Chem*. 1995;270(45):26746–26749.
60. Yu JG, Javorschi S, Hevener AL, et al. The effect of thiazolidinediones on plasma adiponectin levels in normal, obese, and type 2 diabetic subjects. *Diabetes*. 2002;51(10):2968–2974.
61. Guo Y, Li H, Chen X, et al. Novel roles of chloroquine and hydroxychloroquine in Graves' Orbitopathy therapy by targeting orbital fibroblasts. *J Clin Endocrinol Metab*. 2020;105(6):1906–1917.
62. Zhang X, Zhao Q, Li B. Current and promising therapies based on the pathogenesis of Graves' ophthalmopathy. *Front Pharmacol*. 2023;14:1217253.
63. van Koppen CJ, de Gooyer ME, Karstens WJ, et al. Mechanism of action of a nanomolar potent, allosteric antagonist of the thyroid-stimulating hormone receptor. *Br J Pharmacol*. 2012;165(7):2314–2324.
64. Neumann S, Nir EA, Eliseeva E, et al. A selective TSH receptor antagonist inhibits stimulation of thyroid function in female mice. *Endocrinology*. 2014;155(1):310–314.
65. Marcinkowski P, Hoyer I, Specker E, et al. A new highly thyrotropin receptor-selective small-molecule antagonist with potential for the treatment of Graves' Orbitopathy. *Thyroid*. 2019;29(1):111–123.
66. Zeisberg M, Kalluri R. Cellular mechanisms of tissue fibrosis. 1. Common and organ-specific mechanisms associated with tissue fibrosis. *Am J Physiol Cell Physiol*. 2013;304(3):C216–C125.
67. Wynn TA. Cellular and molecular mechanisms of fibrosis. *J Pathol*. 2008;214(2):199–210.
68. Hol EM, Capetanaki Y. Type III intermediate filaments desmin, glial fibrillary acidic protein (GFAP), vimentin, and peripherin. *Cold Spring Harb Perspect Biol*. 2017;9(12):a021642.
69. Patten J, Wang K. Fibronectin in development and wound healing. *Adv Drug Deliv Rev*. 2021;170:353–368.
70. Jankauskiene J, Imbrasiene D. Investigations of ocular changes, extraocular muscle thickness, and eye movements in Graves' ophthalmopathy. *Medicina (Kaunas)*. 2006;42(11):900–903.
71. Dolman PJ. Evaluating Graves' orbitopathy. *Best Pract Res Clin Endocrinol Metab*. 2012;26(3):229–248.
72. Diana T, Holthoff HP, Fassbender J, et al. A novel long-term Graves' disease animal model confirmed by functional thyrotropin receptor antibodies. *Eur Thyroid J*. 2020;9(Suppl 1):51–58.
73. Gong B, Wang C, Meng F, et al. Association between gut microbiota and autoimmune thyroid disease: a systematic review and meta-analysis. *Front Endocrinol (Lausanne)*. 2021;12:774362.
74. Huo D, Cen C, Chang H, et al. Probiotic Bifidobacterium longum supplied with methimazole improved the thyroid function of Graves' disease patients through the gut-thyroid axis. *Commun Biol*. 2021;4(1):1046.
75. Ishaq HM, Mohammad IS, Shahzad M, et al. Molecular alteration analysis of human gut microbial composition in Graves' disease patients. *Int J Biol Sci*. 2018;14(11):1558–1570.
76. Shin NR, Bose S, Wang JH, et al. Chemically or surgically induced thyroid dysfunction altered gut microbiota in rat models. *FASEB J*. 2020;34(6):8686–8701.
77. Zhang M, Yang L, Zhu M, et al. Moutan Cortex polysaccharide ameliorates diabetic kidney disease via modulating gut microbiota dynamically in rats. *Int J Biol Macromol*. 2022;206:849–860.
78. Xu Z, Xiao L, Wang S, et al. Alteration of gastric microbiota and transcriptome in a rat with gastric intestinal metaplasia induced by deoxycholic acid. *Front Microbiol*. 2023;14:1160821.
79. Sun J, Zhao F, Lin B, et al. Gut microbiota participates in antithyroid drug induced liver injury through the lipopolysaccharide related signaling pathway. *Front Pharmacol*. 2020;11:598170.
80. Hu Q, Niu Y, Yang Y, et al. Polydextrose alleviates adipose tissue inflammation and modulates the gut microbiota in high-fat diet-fed mice. *Front Pharmacol*. 2021;12:795483.
81. Zhou C, Zhang W, Lin H, et al. Effect of theaflavin-3,3′-digallate on leptin-deficient induced nonalcoholic fatty liver disease might be related to lipid metabolism regulated by the Fads1/PPARdelta/Fabp4 axis and gut microbiota. *Front Pharmacol*. 2022;13:925264.
82. Liu J, Fu J, Jia Y, Yang N, Li J, Wang G. Serum metabolomic patterns in patients with autoimmune thyroid disease. *Endocr Pract*. 2020;26(1):82–96.
83. Boi F, Pani F, Mariotti S. Thyroid autoimmunity and thyroid cancer: review focused on cytological studies. *Eur Thyroid J*. 2017;6(4):178–186.
84. Lee HY, Sim BC, Nga HT, et al. Metabolite changes during the transition from hyperthyroidism to euthyroidism in patients with graves' disease. *Endocrinol Metab (Seoul)*. 2022;37(6):891–900.
85. Davie JR. Inhibition of histone deacetylase activity by butyrate. *J Nutr*. 2003;133(7 Suppl):2485S–2493S.
86. Segain JP, Raingeard de la Bletiere D, Bourreille A, et al. Butyrate inhibits inflammatory responses through

Investigative Ophthalmology & Visual Science

NFkappaB inhibition: implications for Crohn's disease. *Gut*. 2000;47(3):397–403.

87. Patnala R, Arumugam TV, Gupta N, Dheen ST. HDAC inhibitor sodium butyrate-mediated epigenetic regulation enhances neuroprotective function of microglia during ischemic stroke. *Mol Neurobiol*. 2017;54(8):6391–6411.
88. Khan S, Jena G. Sodium butyrate, a HDAC inhibitor ameliorates eNOS, iNOS and TGF-beta1-induced fibrogenesis, apoptosis and DNA damage in the kidney of juvenile diabetic rats. *Food Chem Toxicol*. 2014;73:127–139.
89. Liu H, Wang J, He T, et al. Butyrate: a double-edged sword for health? *Adv Nutr*. 2018;9(1):21–29.
90. Cavaliere G, Catapano A, Trinchese G, et al. Butyrate improves neuroinflammation and mitochondrial impairment in cerebral cortex and synaptic fraction in an animal model of diet-induced obesity. *Antioxidants (Basel)*. 2022;12(1):4.

Investigative Ophthalmology & Visual Science